Acta Neuropathologica Communications

RESEARCH

Open Access

Microglia drive synaptic and functional connectivity deficits in the Ts65Dn mouse model of Down syndrome by affecting inhibition

Alexia Tiberi[1*], Elena Montagni[2,3], Giulia Borgonovo[1], Eléa Coulomb[1], Laura Restani[2], Anna Letizia Allegra Mascaro[2,3], Simona Capsoni[1,4] and Antonino Cattaneo[1,5]

Abstract

Microglia, the resident immune cells of the brain, play a crucial role in sculpting neuronal circuits during development, and their dysfunction is increasingly implicated in neurodevelopmental disorders such as Down syndrome (DS). Here, we reveal a previously unrecognized pathological mechanism whereby microglia contribute to synaptic and neuronal activity deficits in DS: a selective disruption of microglia–interneuron interactions. Using primary neuron–microglia co-cultures from Ts65Dn mice, we show that while trisomy in neurons drives excitatory synaptic deficits and major microglial morphological changes, microglial trisomy disrupts the regulation of inhibitory synapses in a cell-autonomous manner. To investigate these pathological interactions in vivo, we developed a novel spatial distribution analysis tool that, combined with chemogenetic approaches targeting parvalbumin (PV) interneurons in Ts65Dn mice, allowed us to reveal a disrupted microglia–PV interneuron crosstalk characterized by reduced physical association and impaired microglial responsiveness to PV activity. Finally, by targeting microglia via P2Y12 receptor inhibition, we restored cortical connectivity, rescued PV interneuron function, and improved cognitive performance in Ts65Dn mice. Overall, these findings establish microglia–interneuron dysregulation as a key driver of neuronal activity and synaptic dysfunction in the Ts65Dn mouse model of DS and identify the microglia as a promising therapeutic target to counter circuit dysfunction and cognitive deficits.

*Correspondence:
Alexia Tiberi
alexia.tiberi@sns.it
[1]Bio@SNS Laboratory of Biology, Scuola Normale Superiore, 56126 Pisa, Italy
[2]Institute of Neuroscience, National Research Council, 56124 Pisa, Italy
[3]European Laboratory for Non-Linear Spectroscopy (LENS), 50019 Sesto Fiorentino, Italy
[4]Section of Human Physiology, Department of Neuroscience and Rehabilitation, University of Ferrara, 44121 Ferrara, Italy
[5]Rita Levi-Montalcini European Brain Research Institute (EBRI), 00161 Rome, Italy

Introduction

Down syndrome (DS) is a neurodevelopmental disorder caused by an extra copy of human chromosome 21 (HSA21). Individuals with DS often exhibit learning deficits and memory impairments, particularly in tasks involving working memory, such as verbal or spatial short-term memory [18]. Studies in mouse models have highlighted disruptions in the excitatory/inhibitory (E/I) balance as a key neurodevelopmental alteration in DS, with a specific impairment in parvalbumin (PV) interneuron activity [13]. In particular, studies using the Ts65Dn mouse model have reported altered GABAergic signaling, a delayed developmental GABA switch, and cortical network hyperexcitability [12, 17, 53]—phenotypes that are consistent with the epileptic prevalence in individuals with DS [1]. However, the mechanisms contributing to these inhibitory deficits remain incompletely understood.

Microglia are crucial for brain development and have been increasingly recognized for their role in modulating synaptic plasticity in different ways. They can act by eliminating entire synapses [34, 39]—or affecting synaptic function and size by nibbling parts of presynaptic elements via trogocytosis [49] or by simple contact [9]. Conversely, they can also affect synaptic formation via filopodia induction [29], the release of proplastic neurotrophins [36], or via their ability to sculpt the extracellular matrix, which is an important factor for plasticity processes [14]. Initial research emphasized their role in modulating excitatory synapses [34, 39], but recent findings have also demonstrated their impact on inhibitory networks. For instance, a first account described a negative feedback mechanism in which microglial cells can sense and suppress neuronal activity by detecting ATP via the P2Y12 microglial receptor, thus preventing epileptic-like excessive neurotransmission via the release of adenosine [3]. Moreover, another study found that microglia can phagocytose PV-boutons and affect inhibitory circuitry [19]. Finally, microglia were shown to eliminate inhibitory synapses in a GABA-dependent manner during epilepsy [11].

However, although significant microglial alterations have been reported in mouse models of DS [38], human DS brain tissue [20], and iPSC-based models of human microglia [24], literature addressing the question of whether and how microglia interact *differentially* with inhibitory and excitatory neurons is still lacking. Therefore, it remains unclear whether altered microglial-inhibitory interactions could also directly contribute to DS-related neuronal dysfunction and disrupted E/I balance.

In this study, we aimed to address this knowledge gap by employing neuron-microglia co-culture assays, spatial distribution analyses, chemogenetic manipulations, and wide-field calcium imaging. For this purpose, we employed the Ts65Dn mouse model which, despite its known genetic limitations—namely, partial trisomy for only ~ 65% of HSA21 orthologs and the inclusion of non-HSA21 genes [21], remains one of the most extensively characterized models, particularly with respect to disrupted inhibitory circuitry [12, 17, 53] and microglial alterations [22], making it a relevant system for mechanistic investigation of their relationship. In vitro, we dissected how microglia modulate excitatory and inhibitory connectivity, demonstrating that their impact depends on disease context and microglial genetic background. In vivo, using spatial distribution analyses and chemogenetic approaches, we revealed impaired interactions between microglia and PV interneurons in the Ts65Dn mouse model of DS. Finally, by modulating microglial P2Y12R signaling, we successfully restored functional connectivity, PV interneuron activity, and behavioral outcomes in Ts65Dn mice. Overall, our study clarifies a novel disrupted cellular interaction between microglia and inhibitory neurons in a trisomic context and further points to microglia as an important cellular target to correct neuronal dysfunction and ameliorate cognitive impairments in DS.

Results

Impact of neuronal and microglial genotypes on microglial morphology and phagocytosis in an in vitro *model of Down syndrome*

While the majority of Down syndrome (DS) research has concentrated on how trisomy impacts neuronal physiology [5], the effects of trisomy on microglia remain underexplored. To dissect the respective roles of neuronal and microglial trisomy, we established primary neuron-microglia co-cultures derived from the Ts65Dn mouse model. Since microglial activity is intimately associated with morphological changes [15, 32], we first analyzed how neuronal or microglial trisomy influences microglial morphology (Fig. 1a). Microglial morphological responses were assessed under four conditions: euploid neurons with euploid microglia (nEu + μEu), euploid neurons with trisomic microglia (nEu + μTs), trisomic neurons with euploid microglia (nTs + μEu), and trisomic neurons with trisomic microglia (nTs + μTs). The use of semi-automated morphometric analysis [28], allowed for the semi-automatic segmentation of microglial cells and extraction of various morphological parameters (Fig. 1b, Suppl. Fig. 1a–c, the whole dataset is in Table S1). Principal component analysis (PCA) was initially performed to assess the distribution of the dataset. The density histogram of the four experimental conditions across the first principal component (which accounts for ∿54% of the total variability) suggests that neuronal genotype plays a more critical role in driving morphological differences in

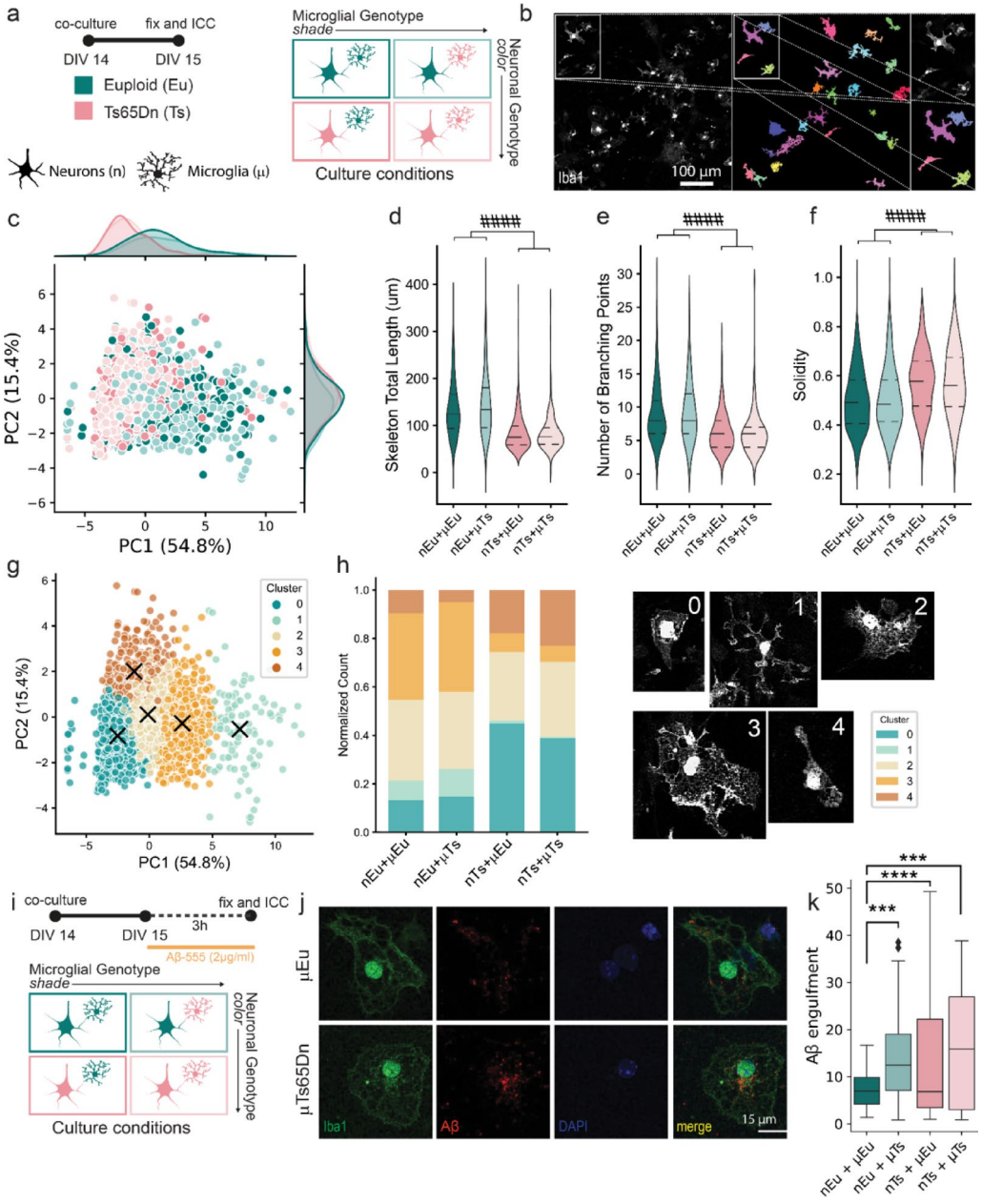

Fig. 1 Impact of neuronal and microglial genotypes on microglial morphology and phagocytosis in an in vitro model of Down syndrome. **a** Primary neuronal and microglial cultures were derived from Euploid (Eu) and Ts65Dn trisomic mice (Ts). Ts or Eu microglia (μ) were plated on top of either Eu or Ts neurons (n) at DIV 14 for 24 h: nEu + μEu; nEu + μTs; nTs + μEu; nTs + μTs. In all figures, color defines neuronal genotype, shade defines microglial genotype. **b** Representative images of the semi-automated segmentation. **c** Scatterplot of all data points on the first two principal components (PC) and their relative marginal distributions. Violin plots of the parameters **d** Skeleton Total Length (Linear Mixed Model (LMM); $F_{Interaction}(1, 2081)$, $p = 0.001$; $F_{Neuronal\ Genotype}(1, 2081)$: $p = 5.57 \times 10^{-73}$), **e** Number of Braching points of the skeletonized microglia (LMM; $F_{Neuronal\ Genotype}(1, 2081)$: $p = 3.77 \times 10^{-38}$), **f** Solidity defined as Area/ConvexArea (LMM; $F_{Neuronal\ Genotype}(1, 2081)$: $p = 5.92 \times 10^{-12}$) (~500 cells per group for 4 replicates). **g** Scatterplot on the PC space showing the distribution of 5 clusters detected by the K-Means clustering algorithm. **h** (left) Barplot showing the abundance of each cluster in each experimental group. (right) Representative images of microglial cells belonging to each cluster (~500 cells per group from 4 replicates). **i** At DIV 15, cocultures were treated for 3 h with Aβ-555, then fixed for ICC. **j** Representative images of the engulfed Aβ material in 2 representative conditions. **k** Box and whiskers plot (10–90 percentile) of the engulfed Aβ-555 in the 4 experimental conditions (LMM; $F_{Interaction}(1, 278)$, $p = 0.014$; $F_{Neuronal\ Genotype}(1, 278)$, $p < 0.0001$; $F_{Microglial\ Genotype}(1, 278)$, $p < 0.0001$); Sidak's multiple comparisons test: nEu + μEu versus nEu + μTs: $p < 0.0001$; nEu + μEu vs; nTs + μEu: $p = 0.0039$; nEu + μEu vs. nTs + μTs: $p = 0.0002$) (~70 cells per group from 4 replicates) (# indicates a significant main effect of a single factor (e.g., neuronal or microglial genotype); * indicates results from post hoc comparisons)

microglia than microglial genotype (Fig. 1c), as the distributions separated by neuronal genotype. Examining individual morphological features, we found that microglia—independent of their genotype—display decreased ramification and morphological complexity when cultured with trisomic neurons. This is indicated by the lower total length of their skeletons (Fig. 1d), decreased number of branching points (Fig. 1e), and increased solidity (see *Methods*; Fig. 1f) (See Suppl. Table 2 for a complete list of all morphological features and their statistical relevance). These results indicate that most morphological alterations in microglia are driven by disease-carrying neurons, with minimal influence from the microglial trisomy. Subsequent K-means clustering of the dataset was used to identify distinct morphological subtypes of microglia (Fig. 1g). Clusters 1 and 3, which correspond to large, ramified cells, were most frequent in microglia cultured with Eu neurons, while Clusters 0 and 4, which represent ameboid microglia, appeared more frequently when microglia were cultured with Ts neurons (Fig. 1h). These findings again underscore a predominant influence of neuronal trisomy on the morphological variability of microglia in Down syndrome. To further investigate the matter from the functional perspective, we then quantified the phagocytic ability of microglial cells toward a fluorescently tagged Aβ peptide (Aβ-555) in the four experimental conditions (Fig. 1i, k). In this assay, both neuronal and microglial trisomy increased the phagocytic activity of microglia toward Aβ-555 (Fig. 1k). Notably, the absence of an additive effect in cultures with both trisomic neurons and microglia (Fig. 1k) suggests that neuronal trisomy may engage shared downstream signaling pathways with microglial trisomy, leading to convergent effects on phagocytosis in this specific assay. These results indicate that while morphological alterations in microglia are primarily driven by the neuronal environment, functional changes in phagocytic capacity can arise from microglial trisomy in a cell-autonomous manner.

The interplay of microglia and neuronal dysfunction in the synaptic deficits in an in vitro *model of Down syndrome*

We then investigated how neuronal and microglial genotypes influence synaptic composition and microglial synaptic engulfment within our co-culture model. In addition to the four experimental groups previously described, we included neuron-only cultures (trisomic: nTs, or euploid: nEu) to establish baseline differences in synaptic marker expression independent of microglial influence. Since microglia have been linked to the modulation of presynaptic puncta when contributing to plasticity [2, 23], we focused our analysis on excitatory ($vGlut1^+$) and inhibitory ($vGAT^+$) presynaptic puncta. Data on the postsynaptic markers (Homer 1b/c; Gephyrin) are presented in Suppl. Fig. 2a-c. Analysis of excitatory presynaptic terminals (vGlut1 puncta area; Fig. 2b, c) demonstrated a clear baseline reduction in synaptic content in trisomic compared to euploid neurons. Interestingly, the effect of microglial genotype on excitatory synaptic content was dependent on neuronal genotype: trisomic microglia (μTs) significantly reduced vGlut1 puncta area when co-cultured with euploid neurons, but this effect was absent in co-cultures containing trisomic neurons. Engulfment assays revealed increased microglial uptake of vGlut1 puncta specifically in co-cultures with trisomic neurons, regardless of microglial genotype, highlighting a critical role of neuronal genotype in promoting excitatory synapse removal (Fig. 2d, e). In contrast, analysis of inhibitory synapses (vGAT+ puncta) highlighted both neuronal and microglial contributions. Trisomic neurons showed a marked reduction in vGAT+ bouton size (Fig. 2f–g), indicating an intrinsic deficit. Additionally, trisomic microglia decreased the size of inhibitory puncta irrespective of the neuronal genotype, suggesting a unique, cell-autonomous dysfunction. This was supported by engulfment analysis showing that μTs microglia displayed enhanced uptake of vGAT+ puncta across conditions (Fig. 2h–i), reinforcing the idea that trisomic microglia selectively drive inhibitory synaptic deficits. Notably, these data also reveal a significant additive effect in co-cultures combining trisomic neurons and trisomic microglia in the context of inhibitory synapse engulfment (Fig. 2i). This contrasts with our Aβ phagocytosis assay (Fig. 1k), where trisomy in one cell type alone appeared sufficient to saturate the response. These findings suggest that cargo-specific differences exist in the way neuronal and microglial trisomy interact to influence microglial engulfment.

To assess the functional impact of these changes, we conducted calcium imaging in selected co-cultures with trisomic neurons (Fig. 2j–k). Interestingly, euploid and trisomic microglia exerted opposite effects on neuronal calcium dynamics. Co-culture with euploid microglia modestly increased the peak amplitude of calcium transients (Fig. 2l) while reducing power in the high-frequency range (1–1.5 Hz), as measured by Fourier analysis (Fig. 2n). In contrast, trisomic microglia increased the power in this frequency band (Fig. 2n) but reduced the integrated calcium signal, as reflected by a decreased area under the curve (AUC) (Fig. 2m). These findings suggest that trisomic microglia shift the temporal dynamics of neuronal calcium activity toward faster, less sustained events—consistent with a perturbation in inhibitory synaptic tone. Overall, while the neuronal trisomy strongly shapes baseline synaptic architecture, trisomic microglia contribute to functional network alterations in a cell-autonomous manner, particularly by disrupting inhibitory balance.

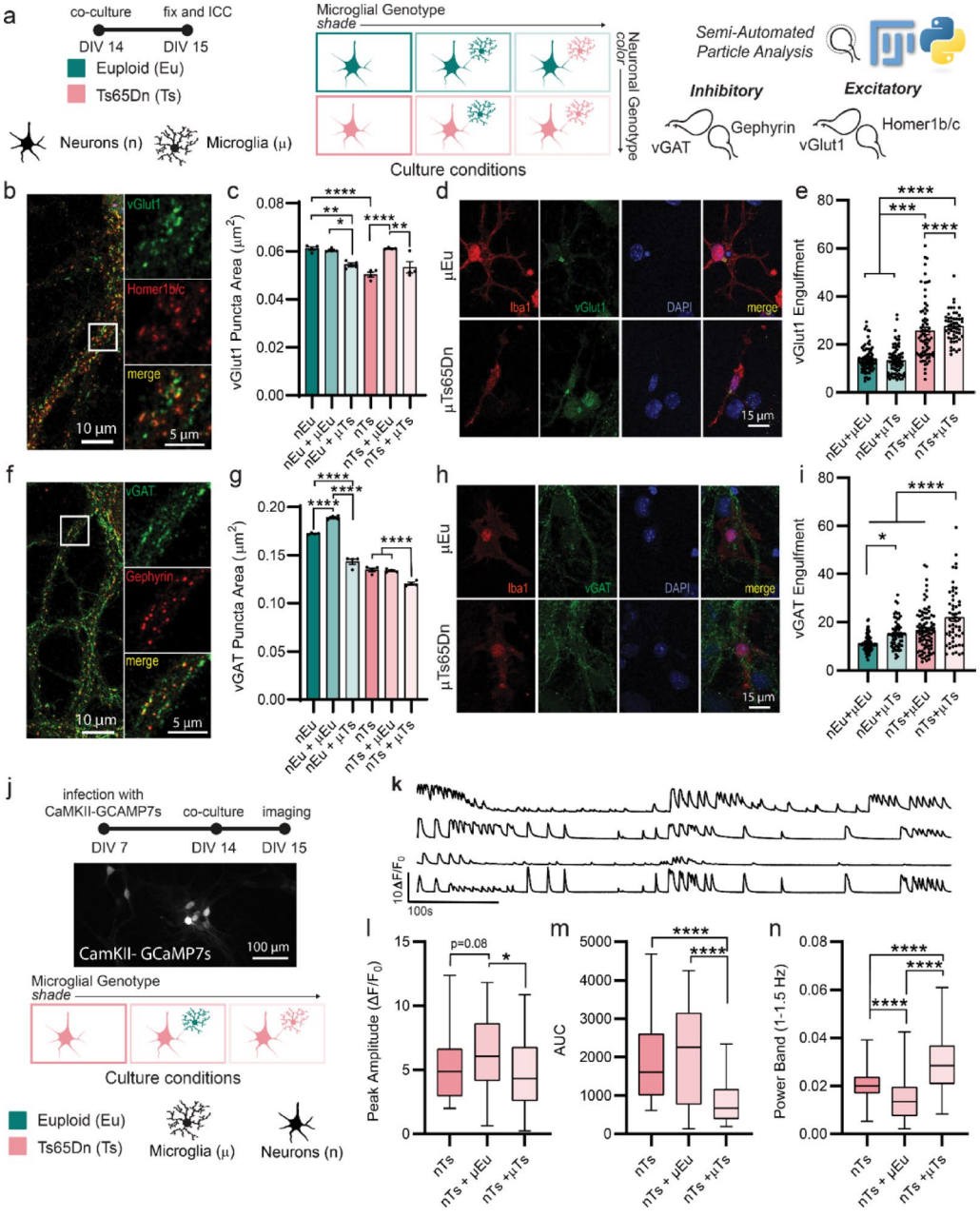

Fig. 2 (See legend on next page.)

Spatial distribution analysis and chemogenetics reveal an impaired PV-microglia interaction in trisomic animals

To investigate the interaction between microglia and neurons in vivo, we decided to start by taking into account their spatial distribution in the somatosensory cortex of 2-month-old Ts65Dn x CX3CR1$^{GFP/+}$ mice. This is of interest as microglia are known to impact plasticity via direct contact [29], and also displace synapses in order to affect neuronal activity [10]. Using immunostaining, we identified microglia (CX3CR1^{GFP}), all neurons (NeuN^{+}), and parvalbumin interneurons (PV^{+}), the most abundant class of cortical interneurons, whose connectivity, importantly for the purpose of this work, is known to be influenced by microglia [19]. PV and NeuN data were then used to distinguish a fourth class of cells composed of mostly excitatory neurons (NeuN^{+} PV^{-}) (Fig. 3a).

First, we analyzed the cell density of these populations, revealing a significant reduction in Iba1^{+} microglia in Ts65Dn, but no change in NeuN^{+} PV^{-} cells or PV^{+} cells. Next, we examined microglia-neuron interactions by analyzing the association of microglia to PV^{+} and NeuN^{+}PV^{-} neurons, categorizing neurons as "microglia-associated" if they fell within a predefined Euclidean distance of microglial somas (Suppl. Fig. 3b). Ts65Dn mice

(See figure on previous page.)

Fig. 2 The interplay of microglia and neuronal dysfunction in determining synaptic deficits in an in vitro model of Down syndrome. **a** Primary neuronal and microglia cultures were derived from Euploid (Eu) and Ts65Dn trisomic mice (Ts). Ts or Eu microglia (μ) were plated on top of either Eu or Ts neurons (n) at DIV 14 for 24 h for a total of 6 experimental conditions (or 4 depending on the assay): nEu, nEu + μEu; nEu + μTs; nTs, nTs + μEu; nTs + μTs. In all figures, color defines neuronal genotype, shade defines microglial genotype. Analysis of puncta markers was performed using a semi-automated analysis using FIJI and Python that allowed for high-throughput results (Suppl. Fig. 2A). **b** Representative images of the vGlut1 and Homer1b/c staining. **c** Barplot of vGlut1 puncta area (Two-way ANOVA, $F_{Interaction}$ (2, 18) = 15.05, $p = 0.0001$; $F_{Neuronal\ Genotype}$ (1, 18) = 16.22, $p = 0.0008$; $F_{Microglial\ Genotype}$ (2, 18) = 19.94, $p < 0.0001$; for the multiple comparisons see Suppl. Table 3 (n = 4 replicates). **d** Representative images of the Iba1-vGlut1 signal used for the engulfment analysis. **e** Barplot of vGlut1 Engulfment (LMM, $F_{Interaction}$ (1, 140), $p = 0.001$; $F_{Neuronal\ Genotype}$ (1, 140), $p < 0.0001$; Tukey's multiple comparisons test: nEu + μEu/nEu + μTs vs. nTs + μTs: $p < 0.001$; nEu + μEu vs. nTs + μEu: $p = 0.0002$) (~ 28–39 cells per group from 3 replicates). **f** Representative images of the vGAT and Gephyrin staining. **g** Barplot of vGAT puncta area (Two-way ANOVA, $F_{Interaction}$ (2, 18) = 95.96, $p < 0.0001$, $F_{Neuronal\ Genotype}$(1, 18) = 270.1, $p < 0.0001$, $F_{Microglial\ Genotype}$ (2, 18) = 233.4, $p < 0.0001$; for the multiple comparisons see Suppl. Table 3 (n = 4 replicates). **h** Representative images of the Iba1-vGAT signal used for the engulfment analysis. **i** Barplot of vGAT Engulfment (LMM; $F_{Interaction}$ (1, 124), $p = 0.0047$; $F_{Microglial\ Genotype}$ (1, 124), $p = 0.0014$; Tukey's multiple comparisons test: nEu + μEu vs. nEu + μTs $p = 0.0125$; nEu + μEu vs. nTs + μTs: $p < 0.0001$; nTs + μEu vs. nTs + μTs: $p < 0.0001$; nEu + μTs vs. nTs + μTs: $p < 0.0001$) (~ 25–39 cells per group from 3 replicates). **j** Neurons were infected at DIV 7 with AAV to express GCaMP7s in CAMKII neurons and imaged at DIV 15. Three experimental groups were used: (i) nTs, (ii) nTs + μEu; (iii) nTs + μTs. **k** Example fluorescent traces extracted from neuronal somata during the 300-s imaging sessions (expressed as ΔF/F0). Box and Whisker plot (Min–Max) of the **l** Peak amplitude (One-way ANOVA, F = 4.335, $p = 0.0143$; Tukey's multiple comparisons test: nTs + μEu vs. nTs + μTs, $p = 0.0108$), **m** Area under the curve (One-way ANOVA, F = 36.50, $p < 0.0001$; Tukey's multiple comparisons test: nTs vs. nTs + μTs, $p < 0.0001$; nTs + μEu vs. nTs + μTs, $p < 0.0001$), and (n) Power Band 1–1.5 Hz which corresponds to the high-frequency band in the Fourier analysis (One-way ANOVA, F = 114.3, $p < 0.0001$; Tukey's multiple comparisons test: nTs vs. nTs + μEu, $p < 0.0001$; nTs vs. nTs + μTs, $p < 0.0001$; nTs + μEu vs. nTs + μTs, $p < 0.0001$) (* indicates results from post hoc comparisons)

displayed reduced percentages of microglia-associated PV^+ and $NeuN^+PV^-$ neurons (Fig. 3c, d, *Observed*). To rule out reduced microglial density as the sole cause of this outcome, we generated a synthetic microglial distribution with preserved density and spacing and recalculated the association between neurons and the synthetic microglia. In this synthetic dataset, the proportion of microglia-associated $NeuN^+PV^-$ neurons was still significantly decreased in Ts65Dn mice compared to controls, indicating that this reduction is, at least in part, density-dependent (Fig. 3c, *Synthetic*). Conversely, for PV^+ interneurons, the loss of interaction in Ts65Dn mice was not observed in the synthetic dataset, suggesting a disease-specific impairment in microglia-PV^+ interneuron interactions that is not attributable to microglial density alone (Fig. 3d, *Synthetic*). A complementary way to look at this is by quantifying the percentage of microglial cells associated with either PV^+ or $NeuN^+PV^-$, which similarly shows a decrease in the percentage of microglial cells that are associated with PV^+ neurons in trisomic animals (Suppl. Fig. 3c, d). To summarize the results, we have then calculated an *E/I association ratio* representing a preference index for microglia for $NeuN^+$ PV^- or PV^+ neurons (See *Methods*). Interestingly, this ratio is increased in trisomic animals (Fig. 3e), suggesting that microglial cells in trisomic animals associate preferentially to excitatory neurons with respect to inhibitory when compared to euploid mice, which could contribute to the E/I imbalance in these mice. We corroborated the E/I unbalance with a puncta-level analysis, where vGlut1 (excitatory) and vGAT (inhibitory) puncta area and density further confirmed a shift toward excitation (Suppl. Fig. 3e–j). Notably, although microglial cells are known to be responsive to sex-specific signals [47], our linear mixed model analysis revealed that sex had little effect only on these parameters (Suppl. Table 3). This indicates that the major driver of microglia-neuron interaction deficits is genotype, with limited contribution from sex, supporting the generalizability of our findings across sexes. We proceeded to explore the potential cause of this decreased association with PV interneurons. We hypothesized that their ability to respond to the GABA neurotransmitter could play a part in this. Microglia's ability to sense and respond to their environment is well documented, particularly their dynamic motility, which has been observed in vivo using two-photon (2p) microscopy [15, 32]. So, to further investigate the pathological interaction between microglia and PV interneurons in DS, we analyzed microglial motility in response to the chemogenetic activation of PV interneurons in euploid and trisomic mice. We injected 2-month-old Ts65Dn x $PV^{CRE/+}$ x $CX3CR1^{GFP/+}$ with either an excitatory DREADD (Gq) or a control viral cocktail (Fig. 3f, g, Suppl. Fig. 3k). Interestingly, in the Gq group, CNO administration triggered a specific decrease in microglial motility in Eu mice, while trisomic mice showed no such response (Fig. 3h). In the control group, CNO administration yielded no change in microglial motility in either group (Fig. 3i). This was most evident in the motility data normalized to baseline (preCNO) (Fig. 3j), where only euploid mice receiving the chemogenetic virus exhibited decreased microglial motility. Overall, our data reveal that in Ts65Dn mice, microglia exhibit impaired interactions with PV interneurons, consistent with our in vitro findings. These results reinforce the idea that pathological microglia-interneuron interactions may contribute to the synaptic and microglial dysfunctions characteristic of Down syndrome.

Functional connectivity deficits in Ts65Dn animals are ameliorated by the inhibition of the microglial P2Y12R

We were then interested in understanding the effect of this miscommunication at the functional level. To this

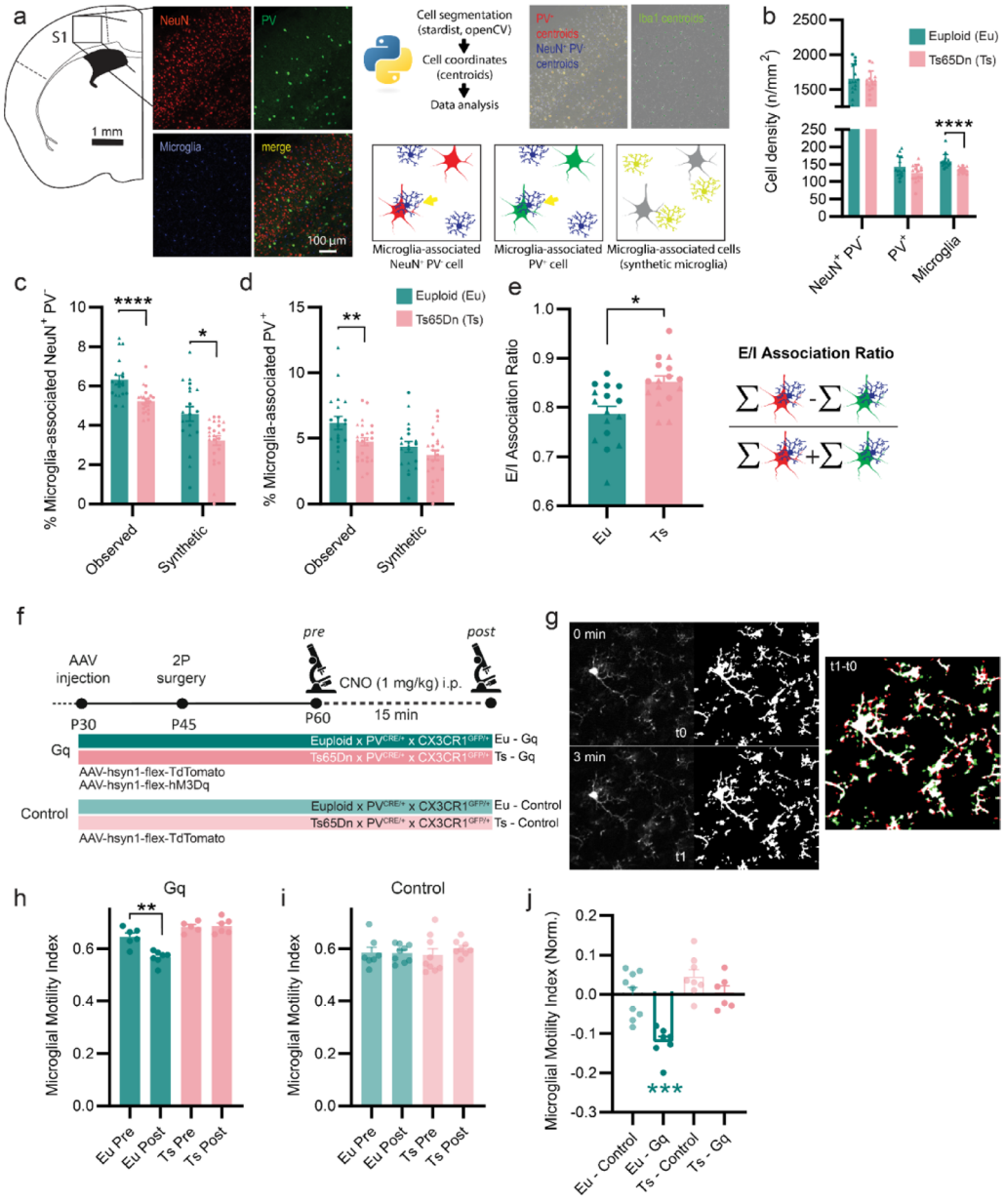

Fig. 3 *Spatial distribution analysis and chemogenetics reveal an impaired PV-microglia interaction in Ts65Dn animals*. **a** PV^+, $NeuN^+$ PV^-, and Microglial cell density and spatial distribution were studied in the somatosensory cortex of P60 euploid (Eu) and trisomic (Ts) Ts65Dn x $CX3CR1^{GFP/+}$ mice. A Python-based image segmentation pipeline powered by the deep learning algorithm Stardist and computer vision packages enabled the precise extraction of cell coordinates of the three populations. Triangles correspond to datapoints coming from female mice, circles to male mice. **b** Cell density of NeuN+ PV-, PV+, and Microglial cells (GFP^+) (Linear Mixed Model; Microglia: $F_{Genotype}$ (1, 31), $p < 0.0001$, F_{Sex} (1, 31), $p = 0.02$). (c) % Microglia-associated $NeuN^+$ PV^- neurons (linear mixed model; observed: $F_{Genotype}$ (1, 31), $p = 0.0017$; synthetic: $F_{Genotype}$ (1, 31), $p = 0.046$). **d** % Microglia-associated PV+ neurons (Linear Mixed Model; Observed: $F_{Genotype}$ (1, 31), $p = 0.0005$). **e** E/I association ratio as defined in the *Methods* section representing the preference of microglia to interact with excitatory over inhibitory neurons (linear mixed model; $F_{Genotype}$ (1, 31), $p = 0.014$) (n = 4 animals per group, 2 per sex with 4 entire cortex analyzed). **f** Triple transgenic mice carrying Cre recombinase in PV interneurons and GFP expression in microglial cells of either euploid (Eu) or trisomic genotype (Ts) were injected with an AAV cocktail of AAV-hsyn1-flex-TdTomato and AAV-hsyn1-flex-hM3Dq (in order to visualize and modulate PV interneurons) or with a control cocktail (AAV-hsyn1-flex-TdTomato). Mice were then implanted for 2p imaging and habituated to the imaging setup. Acquisition of motility was done either at baseline or in response to the injection of CNO (1 mg/kg). **g** Representation of the analysis performed with the imaging data. Z stacks were acquired every 3 min, and a pixel-wise analysis of microglial motility was performed between different time points. The example shown is from a control (euploid) animal. **h** Microglia motility index, defined as the sum of normalized extensions and retractions, in the Gq group that received the chemogenetic virus (Two-way ANOVA, $F_{CNOxGenotype}$ (1, 22) = 5.207, $p = 0.0325$, F_{CNO} (1, 22) = 11.92, $p = 0.0023$, Sidak's multiple comparisons test: Eu vs. Eu + CNO, $p = 0.0007$) (~ 6–8 recording per group from 3 mice). **i** Microglia motility index in the control group that received the control AAV cocktail (Two-way ANOVA). **j** Normalized microglia motility index (One-sample test with Holm-Sidak *p*-value correction, Eu-Gq $p = 0.0008$)

end, we employed mesoscale widefield (WF) calcium imaging to assess cortical Functional Connectivity (FC) of 2-month-old euploid (Eu) and trisomic (Ts) animals (Ts65Dn) either at baseline and after microglia manipulation via the administration of a P2Y12R inhibitor (clopidogrel) (Fig. 4a). P2Y12R is specifically expressed in microglia in the brain (See Suppl. Fig. 4a for the expression in Ts65Dn), and it is known to be involved in regulating different microglial functions, such as their involvement in brain state regulation [27] and plasticity [43, 50].

Using a retro-orbital injection of a blood barrier-permeable virus (AAV-PHP.eB-mCaMKIIα-jGCaMP7f), we selectively transfected excitatory cortical neurons with

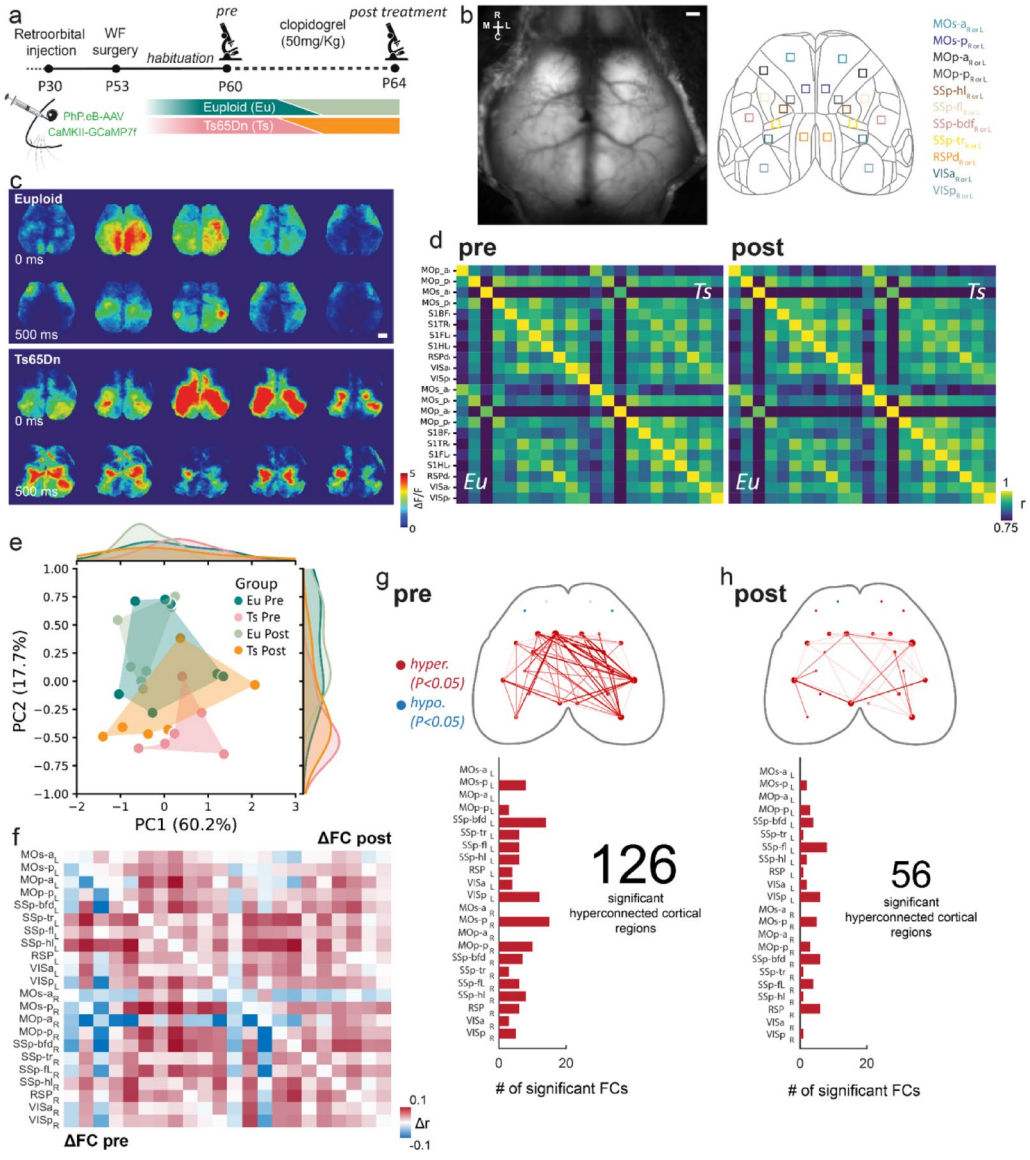

Fig. 4 Functional connectivity deficits in Ts65Dn animals are ameliorated by the inhibition of the microglial P2Y12R. **a** Trisomic (Ts65Dn—Ts) and Euploid (Eu) mice were injected retro-orbitally with a CaMKII-GCaMP7f reporter at P30. At P53, they were subjected to WF surgery and then habituated to being head-fixed under the apparatus for 1 week. Imaging was conducted before and after daily injections of clopidogrel, a P2Y12R inhibitor. **b** Left, representative image of the field of view. Right, cortical parcellation map based on Allen Mouse Brain Atlas. **c** Representative image sequences of calcium activity at the WF in Eu (top) and Ts mice (down). **d** Heatmaps of the average correlation matrices before (pre) and after (post) treatment. Each matrix shows pairwise Pearson correlation coefficients, with Ts mice represented in the upper triangle and euploid Eu mice in the lower triangle. **e** PCA analysis computed on the entire FC maps for all mice (each dot represents a mouse). **f** Matrix of differences in functional connectivity (FC). The lower triangle shows differences between Ts65Dn (Ts) and euploid (Eu) mice at baseline, obtained by subtracting the pre-treatment average FC matrix of Eu mice from that of Ts mice. The upper triangle shows treatment-induced changes in Ts mice, computed by subtracting the pre-treatment average FC matrix of Eu mice from the post-treatment FC matrix of Ts mice. **g**, **h**) Network diagrams of statistically significant ($p < 0.05$) functional alterations in Ts mice compared to Eu animals before treatment (**g**) and after treatment (**h**) with clopidogrel (n = 6 Euploid and 5 Ts65Dn)

a calcium indicator at P30 (Fig. 4b). At P60, we then imaged cortical activity in both Eu and Ts mice (Fig. 4c), computed pairwise correlation coefficients between several cortical regions (Fig. 4d), and compared them between the two groups for evaluating altered network dynamics in Ts65Dn mice before and after Ts's treatment with clopidogrel. Principal component analysis (PCA) of FC data revealed distinct clustering among groups, with Ts65Dn mice showing altered cortical FC compared to euploid controls (Fig. 4e; Ts Pre vs. Eu Pre). Interestingly, clopidogrel treatment in Ts65Dn mice (Ts Post) shifted their connectivity profile closer to that of untreated Eu mice, suggesting a partial restoration of cortical network dynamics.

Given the distinct group clustering observed in the PCA, we next characterized the nature and direction of these alterations. To this end, we applied network-based statistics (NBS) to assess significant changes in FC, identifying patterns of hyper- or hypo-connectivity in Ts65Dn mice relative to Eu controls. Prior to treatment, Ts mice displayed a widespread hyperconnected network (Fig. 4f, g). Following clopidogrel administration, this aberrant hyperconnectivity was markedly reduced (Fig. 4h) by indicating a substantial normalization of excitatory network activity.

Together, these results highlight the potential of microglial modulation to restore cortical network dynamics in Ts65Dn mice via the P2Y12R.

Microglial P2Y12R inhibition ameliorates PV interneuron activity and behavioral performance in Ts65Dn animals

To investigate the effects of P2Y12R inhibition on PV interneuron activity in DS, we performed two-photon calcium imaging in the somatosensory cortex of euploid and Ts65Dn mice expressing GCaMP8m under PV-specific Cre recombinase (PV^{CRE}) (Fig. 5a, b). Imaging of layer IV PV+ interneurons allowed us to extract calcium traces and analyze activity parameters, including peak amplitude, and temporal dynamics in the 1–1.5 Hz range (Fig. 5c). At baseline, Ts65Dn mice displayed reduced power in this frequency band compared to euploid controls, consistent with impaired fast calcium dynamics in PV+ interneurons. Clopidogrel treatment in Ts65Dn mice restored this power band to levels comparable to euploid controls, while no significant changes were observed in peak amplitude across groups (Fig. 5d, e). Importantly, these effects were specific to clopidogrel treatment, as no changes were observed in saline-treated mice, confirming that the normalization of oscillations in Ts65Dn mice was driven by the drug (Fig. 5f, g). Together, these data suggest that clopidogrel selectively enhances PV+ interneuron activity in Ts65Dn mice. To then understand whether these changes brought forth by the inhibition of P2Y12R in microglia could affect behavior, we performed a well-known behavioral task that is known to be affected in Ts65Dn animals [42], the novel object recognition test (NORT, Fig. 5h, i). Before drug treatment, Ts65Dn (Ts) mice showed little preference for the novel object, as indicated by their near-zero discrimination index (DI), whereas Eu controls exhibited a robust DI (Fig. 5k). However, four days of systemic clopidogrel administration significantly rescued recognition memory in Ts mice (Fig. 5m), as shown by their positive DI during the test phase. Both genotypes showed negligible DI differences in the learning phase, indicating similar object exploration during encoding (Fig. 5j, l). No significant effect of sex or interaction with treatment was detected (Suppl. Table 5). These data suggest that P2Y12R inhibition can ameliorate cognitive deficits in Ts65Dn mice. Finally, in this behavioral cohort, we evaluated microglia–neuron spatial associations to find that P2Y12R inhibition restored microglial density, microglial association with PV and with NeuN, and the E/I association ratio (Suppl. Fig. 4b–e), suggesting that targeting microglial-P2Y12R can successfully restore microglial interaction with neurons.

Discussion

Our findings underscore the critical role of microglia in shaping the neuronal deficits associated with Down syndrome (DS), with a particular emphasis on their impact on inhibitory circuits. Significant microglial alterations have been reported in mouse models of DS and DS human brain tissue, and therapeutic interventions targeting these cells have been shown to enhance cognitive functions [20, 38]. For instance, postmortem studies of DS human brain tissues have confirmed elevated microglial activation and inflammatory cytokines [20]. A most recent work using induced pluripotent stem cell (iPSC)-based organoid and chimeric mouse models reported that human DS microglia show an upregulation of interferon-I signaling and over-prune postsynaptic excitatory puncta [24]. Our study explores whether DS microglia differentially affect excitatory and inhibitory circuits and how such interactions could contribute to neuronal dysfunction in DS. By combining in vitro co-culture assays, in vivo imaging, and chemogenetic manipulations, we uncovered distinct microglial contributions to neuronal network dysfunction in DS.

Trisomy in neurons versus trisomy in microglia

One of our central goals was to systematically dissect how trisomy in neurons versus trisomy in microglia differentially contributes to the pathological phenotype in the Ts65Dn mouse model of DS. We, therefore, developed an in vitro experimental pipeline featuring multiple conditions that isolated each variable—neuronal or microglial trisomy—so that we could rigorously compare

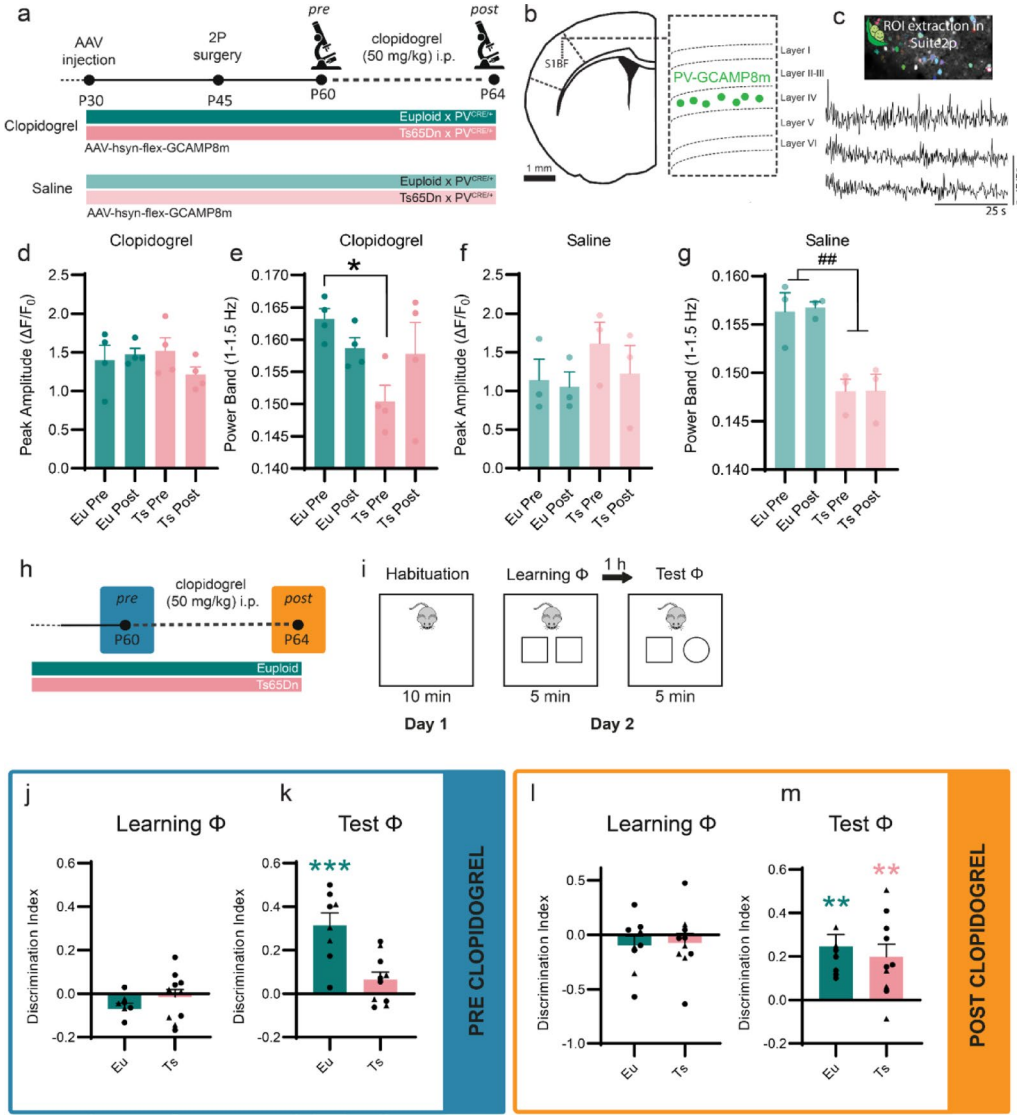

Fig. 5 Microglial P2Y12R Inhibition ameliorates PV interneuron activity and behavioral performance in Ts65Dn animals. **a** P30 Ts65Dn-PVCRE mice were injected in the somatosensory cortex (S1) with an AAV to express GCaMP8m in PV interneurons. At P45, mice underwent cranial window surgery and were allowed to recover for two weeks. Imaging was performed at the two-photon microscope (2P) either before or after treatment with clopidogrel or saline (control). **b** Imaging was performed in S1. **c** Data was extracted using Suite2p, which allows for automatic ROI detection. For the clopidogrel group: **d** Peak amplitude (RM Two-way ANOVA). **e** Power of the 1–1.5 Hz band (RM Two-way ANOVA; $F_{GenotypexTreatment}$ (1, 6) = 4.973.17, $p = 0.06$, Sidak Multiple comparison, Eu Baseline vs. Ts baseline, $p = 0.02$). For the saline-treated group: **f** Peak amplitude (RM two-way ANOVA). **g** Power of the 1–1.5 Hz band (RM Two-way ANOVA; $F_{Genotype}$ (1, 4) = 59.17, $p = 0.0015$) (~6–8 recording per group from 4 mice). **h** Experimental timeline. At P60 ("pre clopidogrel"), mice underwent baseline NORT testing. Clopidogrel (50 mg/kg, i.p.) was administered daily from P60 to P64, and mice were tested again at P64 ("post clopidogrel"). **i** Behavioral design: On Day 1, mice were placed in an open field test (OFT) arena for 10 min (habituation). On Day 2, they first performed the learning phase, consisting of a 5-min exploration of two identical objects. 1 h after the learning phase, mice underwent the test phase (5 min), during which one of the familiar objects was replaced with a novel object. **j**–**m** Discrimination index (mean ± SEM) for EU and Ts mice in the learning and test phases, shown separately for "pre clopidogrel" (**j**, **k**) and "post clopidogrel" (**l**, **m**) (One-sample t-test; PRE: test phase; Eu: $p = 0.0008$; POST: test phase; Eu: 0.0021, Ts: $p = 0.0069$) (n = 9–10 mice per group, circles are datapoints corresponding to males, triangles to females)

their individual effects and possible interactions. This approach allowed us to attribute specific phenomena to each cell type. For instance, changes in microglial morphology and microglia–excitatory presynaptic engulfment were predominantly driven by the trisomic neurons (Fig. 1a–h), likely through altered neuron-derived cues. This is much in line with current literature suggesting that the CNS microenvironment drives microglial identity [6, 25], possibly via the neuronal release of different cytokines, ATP and neurotrasmitters. It is therefore plausible that trisomic neurons secrete altered signaling molecules or fail to provide homeostatic cues necessary to maintain ramified microglial states. In contrast, we identified a novel, cell-autonomous effect of trisomic

microglia on synapse remodeling, particularly in the context of inhibitory synapses. Trisomic microglia showed increased engulfment of vGAT+ terminals and contributed to a global reduction in inhibitory bouton size, consistent with a microglia-driven deficit in inhibitory tone. This may reflect intrinsic, cell-autonomous changes in gene expression or immune priming, highlighting a dissociation between morphology and function in this context which is consistent with the wide repertoire of microglial states that these cells are now known to have [35]. Notably, our VGAT engulfment data also revealed an additive phenotype when both microglia and neurons were trisomic (Fig. 2i), suggesting that their combined dysfunction may exacerbate inhibitory synapse removal through converging or complementary mechanisms. This contrasts with our earlier observation in the Aβ phagocytosis assay (Fig. 1k), where no such additivity was seen—hinting at a cargo-specific regulation of microglial phagocytic behavior. This is in line with current literature on the different molecular mechanisms underlying microglial engulfment of synapses—integrating multiple signals such as complement proteins, P212YR or neuronal distress cues [2, 43]—versus those mediating Aβ phagocytosis (TLR4\CD14 [26] and TREM2 [37]). However, as we did not directly assess the molecular underpinnings of these differential effects, we acknowledge that our interpretation remains speculative and propose this as a hypothesis to be explored in future mechanistic studies. This underscores the complexity of microglial function and supports the idea that phagocytosis cannot be assumed to follow a unitary mode across different substrates or disease states [35].

Although earlier work reported microglial involvement in aberrant excitatory synaptic pruning in DS models [24, 38], our data expand this narrative by highlighting that dysregulation of inhibitory pathways may be at least as significant in driving network dysfunction. This ability of microglia to differentially modulate excitation and inhibition—at the synapse level—depending on disease context, is precisely what could underlie their ability to impinge on the excitatory/inhibitory balance that we know is so important for neurodevelopment and neurodevelopmental disorders. Moreover, our analysis supports the use of neurons and microglia of either genotype when trying to single out microglia-specific effects or novel interactions in an in vitro setting.

Spatial distribution analysis: a novel tool

While our in vitro neuron-microglia co-culture system allowed us to dissect the distinct contributions of neuronal and microglial genotypes to synaptic dysfunction and microglial phenotypes in Down syndrome (DS), it is limited in its ability to fully capture the complexity of the in vivo brain environment. Microglia in the living brain are influenced by a myriad of factors, including interactions with neurons and other glial cells, vascular elements, and systemic signals that are not present in vitro. Transitioning to in vivo studies, we thus sought to assess microglia–neuron interactions within the cortex of Ts65Dn mice. We opted to analyze the somatosensory cortex of these mice as somatosensory processing abnormalities are a common feature of neurodevelopmental disorders, and as such, we thought it could be an interesting candidate for this analysis [4, 7]. To tackle this question in a high-throughput manner, we developed an automated analysis pipeline leveraging modern image segmentation techniques to examine the spatial distribution of three key cell populations: microglia, parvalbumin (PV) interneurons, and predominantly excitatory neurons ($NeuN^{+}PV^{-}$). Given that inhibitory neurons constitute less than 15% of neocortical neurons, and PV+ interneurons account for over 40% of this population [46], we considered the approximation of NeuN+ PV−cells as primarily excitatory to be justified for the purpose of our analysis.

Our approach builds on prior work demonstrating the importance of analyzing microglial distribution at a cellular resolution (e.g., using nearest-neighbor algorithms) [16], and brings it a step further by taking into account neurons. Our pipeline allows for quantification of how microglia associate with different neuronal subtypes, as that might be of interest given existing evidence that microglial contacts can influence neuronal activity [3, 10, 29, 48].

Through this spatial analysis, we detected a specific decrease in the interaction between microglia and PV+ interneurons in the Ts65Dn DS model (Fig. 3). This finding is particularly salient given that microglia play a fundamental role in establishing correct inhibitory connectivity [2, 19], and such a deficit may exacerbate the already compromised inhibitory drive documented in DS or participate in causing it. The chemogenetic experiment further reinforced this conclusion by showing that microglia in Ts65Dn mice failed to respond appropriately to PV^{+} interneuron stimulation, unlike their euploid counterparts. Altogether, these results suggest that altered microglia–PV crosstalk is a central feature of DS pathology. We have made the tool available on GitHub (see *Methods*) in order to allow other scientists to study the relative spatial distribution of microglia and neurons in different brain pathologies, as we believe disruption in such interaction could be a common feature of neurodevelopmental disorders. Moreover, coupling our spatial framework with spatial transcriptomics could help resolve the molecular identity of neurons that associate with microglia, providing deeper insight into whether specific neuronal subtypes are preferentially engaged in microglial interactions.

Importantly, due to technical constraints related to the difficulty of chronic imaging in animals younger than P30, our in vivo data refer to adult mice. It would be of great interest to investigate microglia–PV interneuron interactions during actual neurodevelopment, particularly around P15, when Favuzzi et al. [19] demonstrated a critical role for microglia in shaping PV connectivity. With the current in vivo dataset, we are unable to disentangle whether the observed microglia–PV communication deficits originate during development or emerge later in life.

Widefield calcium imaging in Ts65Dn animals

To gain functional insight into how manipulating microglial phenotypes affects DS-related cognitive deficits, we turned to widefield calcium imaging as a complementary, large-scale readout of cortical activity. Functional connectivity measures—traditionally assessed by fMRI or widefield calcium imaging—have been employed extensively in neurodevelopmental disorder research [52], yet comparable analyses in DS models have been lacking. Notably, Zerbi et al. [51] profiled multiple mouse models of autism and identified at least four distinct "functional connectivity subtypes", with one subtype (cluster 4) characterized by cortical hyperconnectivity linked to microglial dysfunction (e.g., TREM2-deficient mice). Our widefield imaging revealed a similarly hyperconnected cortex in Ts65Dn mice, suggesting potential parallels with other models where microglial abnormalities disrupt normal circuit maturation. While direct comparisons would require using the same imaging modality (e.g., fMRI), these preliminary observations may open avenues for cross-disorder analyses. Moreover, the longitudinal nature of widefield imaging made it feasible to monitor individual mice before and after treatment, strengthening our conclusions about the therapeutic relevance of modulating microglial activity.

Microglial P2Y12R inhibition as a putative treatment for DS cognitive impairment

From a therapeutic standpoint, we show that inhibition of microglial P2Y12R with clopidogrel partially normalizes aberrant hyperconnectivity, restores activity in PV interneurons, and rescues short-term recognition memory (Figs. 4, 5). These outcomes strongly suggest that microglial dysfunction is a contributing factor to E/I imbalance and cognitive impairment in DS. By pharmacologically inhibiting P2Y12R, we may transiently disrupt maladaptive microglial signaling or reset aberrant microglial–interneuron communication, contributing to the observed normalization of network dynamics and behavior. In support of this interpretation, we also observed a restored microglial association with PV+ and NeuN+ neurons, along with normalization of the excitatory/inhibitory (E/I) association ratio in the treated cohort (Supplementary Fig. 4). These findings suggest that P2Y12R signaling may influence not only microglial motility and surveillance but also their spatial relationship with specific neuronal subtypes. Given the receptor's role in sensing purinergic cues such as ATP and ADP, we hypothesize that abnormal P2Y12R activity in trisomic microglia could contribute to mislocalized or excessive interactions with inhibitory neurons, thereby disrupting synaptic architecture. Clopidogrel treatment may counteract these maladaptive interactions and help re-establish balanced microglial–neuronal engagement.

Our findings align with emerging literature positioning P2Y12R as a critical hub in neuron–microglia interactions. For instance, microglial P2Y12R was shown to be essential for experience-dependent synaptic plasticity in the visual cortex during development [43], and for excitatory synaptic transmission in the spinal cord during injury [50]. Most recently, another work revealed that microglial P2Y12R modulates norepinephrine release in a brain state-dependent manner, highlighting its involvement in broader neuromodulatory and arousal-related processes [8].

Further research is needed to define the specificity, timing, and safety of targeting P2Y12R in microglia to target cognitive deficits in DS. A key strength of our study is the convergence of spatial, synaptic, and functional data across in vitro and in vivo platforms. However, the translational interpretation must consider the genetic limitations of the Ts65Dn model, which harbors only ~ 65% of HSA21 orthologs and additional non-HSA21 genes [22]. While it remains a benchmark for studying inhibitory circuit dysfunction in DS [53], future work using more genetically accurate models (e.g., Ts66Yah [19]) will be necessary to generalize these findings. Moreover, identifying more selective microglial modulators or testing interventions across developmental stages may help delineate optimal therapeutic windows. However, the implications of our findings go beyond the specific model used. Our study contributes to a conceptual shift in how microglia are understood within the developing brain. Rather than serving only as passive immune sentinels or sculptors of excitatory synapses, our results position microglia as **dynamic regulators of inhibitory circuitry**—capable of modulating interneuron function and influencing network architecture.

These insights suggest that microglia may play underappreciated roles in other conditions marked by E/I imbalance, including autism spectrum disorders, neurodevelopmental disorders and epilepsy. This in is line with very recent findings showing how microglia can sculpt inhibitory circuits in a GABA-dependent manner in a mouse model of temporal lobe epilepsy, leading to the development of neuronal hyperexcitability [11].

Therefore, while our findings are grounded in the Ts65Ds model of DS, they open broader questions about microglia's involvement in circuit tuning and neurodevelopmental pathology more generally.

Ultimately, our results encourage a broader perspective on neurodevelopmental pathology—one that positions microglia as key contributors to circuit dysfunction and cognitive impairment via their role in shaping inhibitory connectivity.

Methods

Animals

Ts65Dn (Strain #:005252; this particular line lacks retinal degeneration), PVCRE (Strain #:017320), and CX3CR-1GFP (Strain #:005582) mice were obtained from The Jackson Laboratories (Bar Harbor, ME). Genotyping was performed via PCR analysis of ear DNA as specified on The Jackson Laboratories website. All animal experiments complied with the ARRIVE guidelines (Animal Research: Reporting In Vivo Experiments) and adhered to national and international regulations on laboratory animal welfare (EU Directive 2010/63/EU and Italian DL 26 04/03/2014). Mice were housed under a 12-h dark/light cycle with ad libitum access to food and water. The number of subjects used is indicated in the figure legends.

Primary cultures

Primary cortical neurons and glia were prepared at P0, as previously described [44, 45]. Briefly, animals were decapitated, the brain was rapidly excised and placed into ice-cold Hanks Buffered Saline Solution (HBSS; Thermo Fisher Scientific). Brains were kept isolated from one another, and a piece of tissue was kept for genotyping. Cortex was removed and digested for 15 min at 37 °C in HBSS containing 0.1% of trypsin (Thermo Fisher Scientific). Tissue was transferred in culture medium containing 10% FBS and gently disrupted using a flame-polished Pasteur pipette. Following centrifugation at 4 °C for 8 min at 800 r.p.m., the tissue was split to generate both neuronal and glial culture from the same brain. For neuronal cultures, cells were resuspended in fresh DMEM containing 1% Glutamax, 10% FBS, 2% B27 supplement (Gibco, Waltham, MA), 6 mg/ml Glucose, 12.5 mM Glutamate, 10 µg/ml Gentamicin (Gibco) and plated (1.5×10^5 cells/coverslip for a 24-well for immunostaining, or 2×10^5 cells/well for imaging experiments) after proper poly-D-lysine coating (Sigma-Aldrich, St. Louis, MO). Cells were kept at 37 °C in 5% CO_2. After 12–24 h, medium was replaced with Neurobasal A medium (Thermo Fisher Scientific) containing 2% of B27 supplement, 2.5 mM Glutamax, and 10 µg/ml Gentamicin. On the second day, 2.5 mM AraC (Sigma-Aldrich) was added to the medium. For mixed glial cultures, cells were resuspended and maintained in DMEM/F12 containing 1% penicillin/streptomycin, 1% Glutamax and 10% FBS in 5% CO_2 pH 7.4 at 37 °C. they were re-suspended in DMEM/F12 with 1% penicillin/streptomycin, 1% Glutamax, and 10% FBS and plated on the appropriate support 18 h before the experiments. At DIV (days in vitro) 14–16, primary microglia were separated from the mixed primary glial cultures by mild shaking and seeded onto cultured cortical neurons (1×10^5 cells/well). The culture was maintained in Neurobasal-A supplemented with 2% B27, 2 mM L-glutamine, and 10 µg/ml gentamicin and used after 24 h for experiments.

Morphometric analysis of microglia

Co-cultures were fixed in 2% PFA and 5% sucrose for 10 min, washed in PBS, and blocked for 1 h at RT in BSA 1%. Incubation with primary antibody (O.N. 4 °C) was performed at the following concentrations: guinea pig anti-Iba1 1:500 (Synaptic System; #HS-234 308). Images were collected at a Stellaris 8 confocal microscope (Leica) using an HC PL APO CS2 20x/0.75 DRY objective (0.5691034 µm × 0.5691034 µm). Images were processed and analyzed using the published pipeline by Martinez et al. [28] The semi-automatic segmentation allowed for the collection of data for around ~ 500 cells per experimental condition for a total of ~ 2000 cells. In addition to the automatic features generated by the tool (detailed here https://github.com/embl-cba/microglia-morphometry/tree/main), we also derived some of the features suggested by the authors, such as Solidity as Area_Pixel2/ConvexArea_Pixel2, Roundness as Area_Pixel2/EllipsoidLongestAxisRadius_Pixel^2, and Roundness2 as Area_Pixel2/EllipsoidShortestAxisRadius_Pixel^2. Data processing was performed in Python using the following libraries: *numpy* and *pandas* for data handling, *seaborn*, *matplotlib* for data visualization, *scikit-learn* for PCA and K-means clustering, *scipy* and *statsmodels* for statistical analysis. The function *sklearn.StandardScaler* was applied to normalize data before PCA analysis and clustering. The code used to generate figures is available upon request.

Phagocytosis assay

Co-cultures were incubated with fluorescent Aβ-555 (AS-60480-01, ANASPEC) for a final concentration of 2 µg/ml for 3 h, then fixed and processed for immunostaining as in *Morphometric analysis.* Z-stacks of 6 µm corresponding to microglial cells were collected at LSM 900 confocal microscope (Zeiss, Oberkochen, Germany) using a Plan-Apochromat 63x, NA:1.4 oil objective (0.1980717 µm × 0.1980717 × 0.5 µm). Images were processed and analyzed using FIJI (ImageJ) by a blind operator. Briefly, a maximum projection was first computed, and then a ROI corresponding to the microglial cell was manually drawn using the polygon selections tool. The

fluorescence in the Aβ channel was then quantified using the measure function.

Synaptic analysis

Co-cultures were fixed in 2% PFA and 5% sucrose for 10 min, washed in PBS, and blocked for 1 h at RT in BSA 1%. Incubation with primary antibody (O.N. 4 °C) was performed at the following concentrations: guinea pig anti-Homer1bc 1:500 (Synaptic System; #160 023), rabbit anti-vGlut1 1:1000 (Synaptic System; #135 302), mouse anti-Gephyrin 1:1000 (Synaptic System; #147 011), rabbit anti-vGAT 1:1000 (Synaptic System; #131 002). Images corresponding to neuronal dendrites and axons were collected at LSM 900 confocal microscope (Zeiss, Oberkochen, Germany) using a Plan-Apochromat 63x, NA:1.4 oil objective (0.0425353 µm × 0.0425353 × 0.3 µm-for a z depth of 0.9 µm). A custom-made imageJ macro was used to batch process all images together—thus blinding the analysis—using the plugin *Analyze particles,* and save the data in a excel file later imported in python for data analysis. Around 5000—8000 puncta were analyzed per experimental condition. Data is reported as average per experimental replicate.

vGlut1-vGAT engulfment assay

Co-cultures were fixed in 2% PFA and 5% sucrose for 10 min, washed in PBS, and blocked for 1 h at RT in BSA 1%. Incubation with primary antibody (O.N. 4 °C) was performed at the following concentrations: rabbit anti-vGlut1 1:1000 (Synaptic System; #135 302), or rabbit anti-vGAT 1:1000 (Synaptic System; #131 002), and guinea pig anti-Iba1 1:500 (Synaptic System; #234 308). Z-stacks of 6 µm corresponding to microglial cells were collected at LSM 900 confocal microscope (Zeiss, Oberkochen, Germany) using a Plan-Apochromat 63x, NA:1.4 oil objective (0.1980717 µm × 0.1980717 × 0.5 µm). As in the *Phagocytosis assay*, images were processed and analyzed using FIJI (ImageJ) by a blind operator. Briefly, a maximum projection was first computed, and then a ROI corresponding to the microglial cell was manually drawn using the polygon selections tool. The fluorescence in the vGlut1 or vGAT channel was then quantified using the measure function.

In vitro *calcium imaging*

For calcium imaging experiments, after dissection at DIV0 (see *Primary cultures*), Euploid or Trisomic neurons (1×10^6 cells) were plated on WillCo glass-bottom plates (HBST-3512, 12 mm aperture). At DIV7, neurons were infected with AAV-CAMKII-GCaMP7s (v482-PHP.eB, VVF, UZH). Microglia were added on top of the neurons at DIV14, and imaging was performed at DIV15. 20 min before imaging, culture medium was changed with a recording ACSF solution devoid of phenol 120 mM NaCl, 3.5 mM KCl, 0.4 mM KH_2PO_4, 5 mM $NaHCO_3$, 20 mM HEPES, with freshly added 2 mM CaCl2, 4 mM Glucose, 1 mM MgCl2). Widefield time-lapse imaging was conducted at 3 Hz for 3 min using a Zeiss confocal microscope with a 10 × objective, resulting in a final pixel size of 0.548 × 0.548 µm. Fluorescent traces of the neuronal somata were extracted using suite2p [33] (fs = 3, tau = 2), data was then processed in Python for subsequent analysis. In particular, we derived the ΔF/F0 using as F0 the 10th percentile, the peak amplitude by simply outputting the max value of the ΔF/F0 trace, the area under the curve and Fourier transform by using *scipy*'s functions *integrate* and *fft*. The resulting Fourier power spectrum was divided by looking at power under 1 Hz and between 1 to 1.5 Hz (which is the maximum allowed by the Nyquist theorem). Graphpad Prism was then used to plot the data. The functions created to analyze the data will be made available upon acceptance of the manuscript.

Immunofluorescence of brain slices

As previously described[44], mice received terminal anesthesia (chloral hydrate, 10 mg/kg), they were perfused with PBS, 4% paraformaldehyde/PBS, postfixed O.N. and stored at 4 °C until sectioning. 50 µm coronal sections were cut using a microtome (Leica Microsystems, Wetzlar, Germany). After 2 h of blocking in 10% BSA + 0.5% Triton-X-100 in PBS, sections were incubated with a mix of primary antibodies in 1% BSA + 0.05%Triton-X-100 in PBS overnight at 4 °C. Microglia were stained with rabbit anti-Iba1 1:500 (Wako, Osaka, Japan, 019–19741), or guinea pig anti-Iba1 1:500 (Synaptic System; #234 308); PV cells were stained using the rabbit anti-Parvalbumin antibody (Swant; #PV27a, 1:1000), NeuN cells with anti-guinea pig Anti-NeuN purified Antibody (1:1000, Sigma-Aldrich; #ABN90P). Sections were then incubated for 2 h at RT with the appropriate secondary antibody (Thermo Fisher Scientific; A-21428 diluted 1:500). Images were collected at a Stellaris 8 confocal microscope (Leica) using an HC PL APO CS2 20x/0.75 DRY objective or a Plan-Apochromat 63x, NA:1.4 oil objective. Using a similar protocol, for P2Y12R staining the primary antibody used was Synaptic System; #476 011.

Spatial distribution analysis PV-microglia

Single plane acquisitions (0.7575756 µm × 0.7575756 µm) corresponding to the somatosensory cortex were acquired for both PV, NeuN, and Microglia (GFP positive because of the $CX3CR1^{GFP/+}$) channels as defined in *Immunofluorescence of brain slices*. Segmentation and the determination of all x, y coordinates for all channels were performed in Python. For Microglia and PV cells which are quite sparse, a computer vision approach was used using openCV DOG filtering. For NeuN, *stardist* (https:

//github.com/stardist/stardist) was used to detect all cells [40]. We analyzed 4 mice per group (euploid vs trisomic—Ts65Dn) and from each mouse we analyzed 4 different brain slices containing S1 counting per mouse ~ 1000 Microglial cells, ~ 16,000 NeuN+ cells, ~ 2000 PV+ cells (so in total overall we segmented 15,000 Microglial cells, 9000 PV+ cells, and more that 100,000 NeuN+ cells). NeuN+ PV- cells were computed by looking at the proximity of PV and NeuN centroids in order to eliminate PV+ cells from the dataset. We then proceed to analyze the relative spatial distribution of these populations. Briefly, the Euclidean distance of each PV or NeuN with any microglia cell was first calculated *scipy.spatial* function *distance*. The Average Nearest Distance (AND) was defined as the average distance between a neuron and its closest microglia. Microglia-associated neurons were defined as those neurons that had a microglial cell within 15 pixels (~ 11 µm) of their centroids (the results are reported as percentage over the total number of neurons). As a control for all parameters, a synthetic dataset of microglia coordinates was computed (synthetic), so to maintain the same number of microglia in the space with a similar average distance between microglia as the observed dataset (to allow for some natural tiling). We also computed the complementary % PV-associated Microglia as (n. of PV-Associated Microglia)/(n. microglia) and the % $NeuN^+PV^-$-associated Microglia. We also calculated the AND between microglia and their closes PV or NeuN+ PV- cells. As an interesting derivative parameter, we also computed the E/I Association Ratio as (% $NeuN^+PV^-$-associated Microglia—% PV-associated Microglia)/(% $NeuN^+PV^-$-associated Microglia + % PV-associated Microglia) to measure the preference of microglia for associating with either PV^+ or $NeuN^+PV^-$ neurons. All code created for the analysis (from segmentation to data analysis) can be found here (https://github.com/AlexiaTiberi/MicroNeuSeg) and here (https://zenodo.org/records/15228611). In this manuscript, we highlight some of the best parameters that came out of the analysis, but we report all the statistics for all parameters in Suppl. Table 3.

AAV and 2P surgery

Ts65Dn x $CX_3CR\text{-}1^{GFP}$ x PV^{CRE} were injected in the somatosensory cortex (+ 2.2–2.5 mm lateral, + 0.5 mm bregma, 0.5 mm deep) at P30 with an AAV cocktail (VVF, ETH, Zurich) containing a 1:5 of AAV9/2-hsyn1-dlox-tdTomato (v284-9) and a 4:5 of either saline (Control Group) or AAV9-hsyn1-dlox-hM3D(Gq)_mCherry (v89-9) (Gq group) in order to visualize and chemogenetically control the activity of PV interneurons. Ts65Dn x PV^{CRE} were instead injected with an AAV9-hSyn1-dlox-jGCaMP8m (v628-9) in the same coordinates. Two weeks after injection, mice underwent craniotomy and head-fixation implant surgery. Briefly, mice were anesthetized with zoletil-xylazin (80–10 mg/kg, i.p.). Dexamethasone (subcutaneous 0.2 mg/kg) and Lidocaine (2%, 15–20 µL, subcutaneous, scalp area) were administered. The scalp was first cleaned with iodine, shaved, and a large portion of the skin covering both hemispheres was removed. The skull was thoroughly cleaned with a scalpel blade. A 3 mm circular craniotomy was drawn and thinned using the AAV injection coordinates as a guide, and bone was replaced with a 3 mm coverslip using cyanoacrylate as a fixative. A metal head-plate was fixed to the skull with dental cement (Super-Bond), and the skull and head-plate were further covered with additional cement to complete the surgery. The animals were allowed to recover in a heated box. Mice were left to recover for 14–20 days to reduce inflammation in the surgical area, thereby improving optical access to the tissue.

2P imaging

Imaging was performed using a Bruker Ultima Investigator™ microscope equipped with a GaSsP Photomultiplier tube and controlled by the scanning software Prairie View. Laser excitation was provided by a tunable Ti:Sapphire pulsating LASER (Chameleon Ultra™, Coherent) tuned at 920 nm and excitation power was controlled with a Pockels Cell. LASER power was maintained under a maximum of 40 mW on the sample. For 2P imaging of microglia motility, the analysis was done in anesthetized animals. Using a 20 × long WD water immersion objective (Olympus XLUMPlanFL N 20 × N.A. = 1.00), z-stacks of 100 µm every 3 min were acquired (512 × 512 pixels, x–y resolution: 0.23 µm/px, z step: 1 µm, 4 × zoom). CNO was then injected i.p. (1 mg/kg) and after 15 min, zstacks were yet again acquired for around 30 min. For calcium imaging of PV interneurons, timelapse recordings of a single plane (5 min) containing PV+ somas were acquired in spiral mode (fps: 4 Hz, 256 × 256 pixels, x–y resolution: 1.8 µm/px).

2P data analysis

For microglial motility analysis, we extracted single planes from all time points analyzed so that the same microglia were present at each time point in Fiji. The corresponding tiff was registered in Fiji using LInear Stack Alignment with SIFT plugin, to eliminate the x,y drift. The tiff was then saved and imported into Python using *tifffile* for analysis. Briefly, The analysis consisted of a normalization step (*cv2.normalize*), subtraction of background (*skimage white_tophat*) a denoise step using a Gaussian filter (*cv2.GaussianBlur*). Images were then thresholded to get binary images (*cv2.threshold*), which were used to compute the pixel-wise difference at each time point. For example, t0 and t1 are consecutive time

points. *Extensions* are the pixels that are present in t1 but not t0, *retractions* are those that are in t0 and not in t1. We counted all *extensions* and *retractions* and normalized them for the total number of pixels at each time point (to account for changes in fluorescence). The *microglial motility index* is the sum of normalized *extensions* and *retractions*. For calcium imaging of PV interneurons, single traces were extracted using the python package suite2p, then the.npy file was imported into python for data analysis. The deltaF/F0 was computed using as F0 the 5 percentile of the entire fluorescent trace. Peak amplitude, AUC, and Fourier analysis were performed as those for In Vitro *Calcium Imaging.*

Wide-field imaging

Surgery: P30 Ts65Dn and euploid mice were injected retro-orbitally with a genetically encoded calcium indicator. Briefly, the virus (ssAAV-PHP.eB/2-mCaMKIIα-jGCaMP7f-WPRE-bGHp(A)) (1.3 × 10E13 vg/ml, volume: 50µL, v493-PHP.eB, Viral Vector Facility, ETH, Zurich) diluted in 100µL of saline solution was intravenously injected in the retro-orbital sinus of mice under isoflurane anesthesia (final volume of 150µL) to allow wide-brain infection. Two weeks after AAV injection, mice underwent an intact-skull preparation to provide direct optical access to the cortex (modified from Montagni et al.[30]). The surgery was performed under a cocktail of ketamine/xylazine (100/10 mg/kg i.p.). The skin and the periosteum were removed. Bregma was marked for stereotactic reference. A custom-made aluminum head-bar placed behind lambda was glued to the skull using transparent dental cement (Super Bond C&B–Sun Medical). The exposed skull was then covered with a thin layer of the same cement.

Wide-field microscopy setup: Imaging was performed on the intact skull of the awake head-fixed animal using a custom-made microscope setup. To excite the GCaMP7f indicator, a 470 nm light beam (LED, M470L3, Thorlabs) filtered by a bandpass filter (469/17.5 nm, Thorlabs) is directed by a dichroic mirror (MD498, Thorlabs) onto the objective lens (TL2X-SAP 2X Super Apochromatic Microscope Objective, 0.1 NA, 56.3 mm WD, Thorlabs). Reflectance images were acquired using a light source positioned at 45° incident to the brain surface (530 nm LED light, M530L4; Thorlabs, New Jersey, United State). Stroboscopic illumination (25 Hz/LED) was used. The fluorescence and reflectance signals was selected by a bandpass filter (525/50 nm filter, Semrock, Rochester, New York, USA) and collected by a CMOS camera (ORCA-Flash4.0 V2 Digital CMOS camera/C11440-22CU, Hamamatsu). Images are acquired with 9 ms exposure time for 6000 total frames with a resolution of 512 × 512 pixels and a field of view (FOV) of 1.15 × 1.15 cm (depth 16-bit).

Habituation and awake imaging: One week after the surgery mice were acclimated to the head-fixation for 5–4 days (10 min a day/mouse) to gradually reduce anxiety and abrupt movements prior to data collection. Head-fixed imaging sessions were performed before and after the systemic injection of the P2Y12R inhibitor, clopidogrel (50 mg/kg). Each imaging session involves 5 recordings (120 s-long) of spontaneous cortical activity in awake, resting-state mice.

Image processing and data analysis: All analyses were performed in MATLAB. Each imaging session was registered using custom-made software, by taking into account the bregma and λ position. An animal-specific field of view template was used to manually adjust the imaging field daily. To dissect the contribution of each cortical area, we registered the cortex to the surface of the Allen Institute Mouse Brain Atlas (www.brain-map.org) projected to our plane of imaging. For each block, image stacks were processed to obtain the estimates of ΔF/F0. ΔF/F0 was computed for each pixel by using the equation ΔF/F0 = (F−F0)/F0, with F representing fluorescence at a given time and F0 the mean fluorescence [30]. Hemodynamic correction was performed as described by Scott and colleagues [41]. Briefly, using the ratiometric approach:

$$\frac{F}{F_0} = \frac{\frac{I^{482}}{I_0^{482}}}{\frac{I^{525}}{I_0^{525}}}$$

The field of view was then downsampled to 128 × 128 pixels. For analyzing FC, a total of 22 ROIs were selected (11 ROI for each hemisphere, 5 × 5 pixels) representing key cortical regions. Correlation mapping was done for each subject by computing Pearson's correlation coefficient between the average signals extracted from each ROI, with that of each other ROI. The single-subject correlation maps were transformed using Fisher's r-to-z transform and then averaged across all animals. Averaged maps were re-transformed to correlation values (r-scores) for figure purpose. For each mouse, r(euploid)-r(Ts65Dn) was calculated and averaged across mice in order to visualize matrices of difference between the two groups. ROIs positions in FC graphs were arranged according to their anatomical coordinates. Lines and symbol sizes represented the level of correlated FC and the number of such connections associated with the ROI, respectively.

The abbreviations and extended names for each areas are as follows: MOs-a, anterior region of secondary motor cortex; MOs-p, posterior region of secondary motor cortex; MOp-a, anterior region of primary motor cortex; MOp-p, posterior region of primary motor cortex; SSp-bfd, primary somatosensory area, barrefield; SSp-tr, primary somatosensory area, trunk; SSp-fL,

primary somatosensory area, forelimb; SSp-hl, primary somatosensory area, hindlimb; RSP, retrosplenial cortex; VISa, associative visual cortex; VISp, primary visual cortex. Throughout the text and figures, suffixes L and R were added to denote cortical areas of the left or right hemisphere, respectively (e.g., RSP_L, RSP_R).

Statistical analysis: Network Based Statistic (NBS) Toolbox in MATLAB was used to statistically assess functional network connectivity [31]. We tested for both significantly higher and lower correlations. Differences were considered significant at $p < 0.05$.

Behavioral analysis

We employed the Novel Object Recognition Test (NORT) to evaluate the effect of our treatment. On day 1, mice were habituated to the testing arena for 10 min. On day 2, mice underwent a familiarization session with two identical objects (learning phase), followed one hour later by a test session in which one familiar object was paired with a novel one (test phase). The same day, mice received the first of four daily treatments with clopidogrel. The day after the last injection, mice repeated the habituation session (10 min). On the subsequent day, mice performed another learning and test session, using a completely new set of objects distinct from those used prior to treatment. The preference for the novel object was calculated using the **preference index**, defined as: (time exploring novel object – time exploring familiar object) / (total exploration time). Analysis was conducted using the automatic tracking program EthoVision (Noldus), where a circular ROI was drawn around the object, and detection occurred when the animal's nose entered the ROI.

Statistical analysis

Data are displayed as individual dots and mean ± SEM, violin plot or box plots (using *seaborn* functions *sns.violinplot* or *sns.boxplot*). Normality was assessed using the D'Agostino & Pearson test in GraphPad. Analysis of factors was performed using Linear Mixed Models when having to account for repeated measures in a sample, while two-way ANOVA was preferred when analyzing animal or experimental replicate means.

Linear mixed-effects model (LMM) were fitted to account for fixed effects (such as Genotype, Sex, or the genotype of the two cell populations in vitro), as well as their interaction. A random intercept was included to account for repeated measures (multiple measurements per animal or per experimental replicate in vitro). The model parameters were estimated using the 'powell' optimizer which performs well with a low number of replicates. When reporting the effect of factors, we used the syntax F_{factor}(degrees of freedom (df), number of replicates—df). Statistical significance was defined at $p < 0.05$. Differences were considered to be significant if $p < 0.05$ and are indicated by *; those at $p < 0.01$ are indicated by **; those at $p < 0.001$ are indicated by ***; those at $p < 0.0001$ by ****. When reporting the effect of single factors (ANOVA, ANCOVA or LMM) we used # instead of *. Comparisons between two groups following a Normal distribution were analyzed using an unpaired t-test (two-tail distribution). Statistical analysis was either performed using GraphPad Prism (Graph-Pad Software) or python's *scipy* and *statmodels*.

Supplementary Information

The online version contains supplementary material available at https://doi.org/10.1186/s40478-025-02189-4.

Supplementary Material 1.

Supplementary Material 2.

Supplementary Material 3.

Acknowledgements

We would like to thank the Jerome Lejeune Foundation that supported this research via a Postdoctoral fellowship to AT named "Microglial cells as contributors to the excitatory/inhibitory balance: a key to understand epileptic prevalence in Down syndrome." We would also like to thank the entire team at IN-CNR and SNS: Sara Cornuti, Valentino Totaro, Stefano Guglielmo, Antea Minetti, Beatrice D'Orsi, Claudia Alia, Cristina Spalletti for scientific advice, Maria Antonietta Calvello, Vania Liverani, Renzo Di Renzo, and Elena Novelli for technical support, Cecilia Ciampi, Sara Ciampi, and Francesca Biondi for the animal care.

Author contributions

Conceptualization, A.T., L.R., S.C., and A.C.: methodology, A.T., G.B., E.M., A.L.A.M.; software, A.T. and E.M.; formal analysis, A.T. and E.M.; investigation, A.T., G.B., E. C., and E.M.; resources, A.T., S.C., A.C., and A.L.A.M.; data curation, A.T., E.M.; writing—original draft, A.T.; writing—review and editing, A.T., G.B., E.M., E. C., A.L.A.M., L.R., S.C., and A.C. visualization, A.T., E.M.; supervision, A.T., A.L.A.M., L.R., S.C., and A.C.; project administration, A.T.; funding acquisition, A.T.

Funding

This work was funded by a postdoctoral fellowship to AT named "Microglial cells as contributors to the excitatory/inhibitory balance: a key to understand epileptic prevalence in Down syndrome.".

Data availability

All code created for the spatial distribution analysis (from segmentation to data analysis) can be found here (https://github.com/AlexiaTiberi/MicroNeuSeg) and here (https://zenodo.org/records/15228611).

Declarations

Ethics approval and consent to participate

Not applicable.

Consent for publication

Not applicable.

Competing interests

The authors declare no competing interests.

Received: 2 July 2025 / Accepted: 15 November 2025
Published online: 17 December 2025

References

1. Altuna M, Giménez S, Fortea J (2021) Epilepsy in Down syndrome: a highly prevalent comorbidity. J Clin Med 10 2776. https://doi.org/10.3390/jcm10132776
2. Andoh M, Shinoda N, Taira Y, Araki T, Kasahara Y, Takeuchi H, Miura M, Ikegaya Y, Koyama R (2025) Nonapoptotic caspase-3 guides C1q-dependent synaptic phagocytosis by microglia. Nat Commun 16:1–18. https://doi.org/10.1038/s41467-025-56342-7
3. Badimon A, Strasburger HJ, Ayata P, Chen X, Nair A, Ikegami A, Hwang P, Chan AT, Graves SM, Uweru JO, Ledderose C, Kutlu MG, Wheeler MA, Kahan A, Ishikawa M, Wang Y-C, Loh Y-HE, Jiang JX, Surmeier DJ, Robson SC, Junger WG, Sebra R, Calipari ES, Kenny PJ, Eyo UB, Colonna M, Quintana FJ, Wake H, Gradinaru V, Schaefer A (2020) Negative feedback control of neuronal activity by microglia. Nature 586:417–423. https://doi.org/10.1038/s41586-020-2777-8
4. Balasco L, Pagani M, Pangrazzi L, Chelini G, Viscido F, Chama AGC, Galbusera A, Provenzano G, Gozzi A, Bozzi Y (2022) Somatosensory cortex hyperconnectivity and impaired whisker-dependent responses in Cntnap2 mice. Neurobiol Dis 169:105742. https://doi.org/10.1016/j.nbd.2022.105742
5. Bartesaghi R (2023) Brain circuit pathology in Down syndrome: from neurons to neural networks. Rev Neurosci 34:365–423. https://doi.org/10.1515/revneuro-2022-0067
6. Bennett FC, Bennett ML, Yaqoob F, Mulinyawe SB, Grant GA, Hayden Gephart M, Plowey ED, Barres BA (2018) A combination of ontogeny and CNS environment establishes microglial identity. Neuron 98:1170-1183.e8. https://doi.org/10.1016/j.neuron.2018.05.014
7. Brandes-Aitken A, Powers R, Wren J, Chu R, Shapiro KA, Steele M, Mukherjee P, Marco EJ (2024) Sensory processing subtypes relate to distinct emotional and behavioral phenotypes in a mixed neurodevelopmental cohort. Sci Rep 14:29326. https://doi.org/10.1038/s41598-024-78573-2
8. Cao K, Qiu L, Lu X, Wu W, Hu Y, Cui Z, Jiang C, Luo Y, Shao Y, Xi W, Zeng L-H, Xu H, Ma H, Zhang Z, Peng J, Duan S, Gao Z (2023) Microglia modulate general anesthesia through P2Y12 receptor. Curr Biol 33:2187-2200.e6. https://doi.org/10.1016/j.cub.2023.04.047
9. Cheadle L, Rivera SA, Phelps JS, Ennis KA, Stevens B, Burkly LC, Lee W-CA, Greenberg ME (2020) Sensory experience engages microglia to shape neural connectivity through a non-phagocytic mechanism. Neuron 108:451-468.e9. https://doi.org/10.1016/j.neuron.2020.08.002
10. Chen Z, Jalabi W, Hu W, Park H-J, Gale JT, Kidd GJ, Bernatowicz R, Gossman ZC, Chen JT, Dutta R, Trapp BD (2014) Microglial displacement of inhibitory synapses provides neuroprotection in the adult brain. Nat Commun 5:4486. https://doi.org/10.1038/ncomms5486
11. Chen Z-P, Zhao X, Wang S, Cai R, Liu Q, Ye H, Wang M-J, Peng S-Y, Xue W-X, Zhang Y-X, Li W, Tang H, Huang T, Zhang Q, Li L, Gao L, Zhou H, Hang C, Zhu J-N, Li X, Liu X, Cong Q, Yan C (2025) GABA-dependent microglial elimination of inhibitory synapses underlies neuronal hyperexcitability in epilepsy. Nat Neurosci. https://doi.org/10.1038/s41593-025-01979-2
12. Contestabile A, Magara S, Cancedda L (2017) The GABAergic hypothesis for cognitive disabilities in Down syndrome. Front Cell Neurosci 11:54. https://doi.org/10.3389/fncel.2017.00054
13. Costa ACS, Scott-McKean JJ (2013) Prospects for improving brain function in individuals with Down syndrome. CNS Drugs 27:679–702. https://doi.org/10.1007/s40263-013-0089-3
14. Crapser JD, Arreola MA, Tsourmas KI, Green KN (2021) Microglia as hackers of the matrix: sculpting synapses and the extracellular space. Cell Mol Immunol 18:2472–2488. https://doi.org/10.1038/s41423-021-00751-3
15. Davalos D, Grutzendler J, Yang G, Kim JV, Zuo Y, Jung S, Littman DR, Dustin ML, Gan W-B (2005) ATP mediates rapid microglial response to local brain injury in vivo. Nat Neurosci 8:752–758. https://doi.org/10.1038/nn1472
16. Davis BM, Salinas-Navarro M, Cordeiro MF, Moons L, De Groef L (2017) Characterizing microglia activation: a spatial statistics approach to maximize information extraction. Sci Rep 7:1576. https://doi.org/10.1038/s41598-017-01747-8
17. Deidda G, Parrini M, Naskar S, Bozarth IF, Contestabile A, Cancedda L (2015) Reversing excitatory GABAAR signaling restores synaptic plasticity and memory in a mouse model of Down syndrome. Nat Med 21:318–326. https://doi.org/10.1038/nm.3827
18. Dierssen M (2012) Down syndrome: the brain in trisomic mode. Nat Rev Neurosci 13:844–858. https://doi.org/10.1038/nrn3314
19. Favuzzi E, Huang S, Saldi GA, Binan L, Ibrahim LA, Fernández-Otero M, Cao Y, Zeine A, Sefah A, Zheng K, Xu Q, Khlestova E, Farhi SL, Bonneau R, Datta SR, Stevens B, Fishell G (2021) GABA-receptive microglia selectively sculpt developing inhibitory circuits. Cell 184:4048-4063.e32. https://doi.org/10.1016/j.cell.2021.06.018
20. Flores-Aguilar L, Iulita MF, Kovecses O, Torres MD, Levi SM, Zhang Y, Askenazi M, Wisniewski T, Busciglio J, Cuello AC (2020) Evolution of neuroinflammation across the lifespan of individuals with Down syndrome. Brain 143:3653–3671. https://doi.org/10.1093/brain/awaa326
21. Gupta M, Dhanasekaran AR, Gardiner KJ (2016) Mouse models of Down syndrome: gene content and consequences. Mamm Genome 27:538–555. https://doi.org/10.1007/s00335-016-9661-8
22. Hamlett ED, Hjorth E, Ledreux A, Gilmore A, Schultzberg M, Granholm AC (2020) RvE1 treatment prevents memory loss and neuroinflammation in the Ts65Dn mouse model of Down syndrome. Glia 68:1347–1360. https://doi.org/10.1002/glia.23779
23. Hashimoto A, Kawamura N, Tarusawa E, Takeda I, Aoyama Y, Ohno N, Inoue M, Kagamiuchi M, Kato D, Matsumoto M, Hasegawa Y, Nabekura J, Schaefer A, Moorhouse AJ, Yagi T, Wake H (2023) Microglia enable cross-modal plasticity by removing inhibitory synapses. Cell Rep 42:112383. https://doi.org/10.1016/j.celrep.2023.112383
24. Jin M, Xu R, Wang L, Alam MM, Ma Z, Zhu S, Martini AC, Jadali A, Bernabucci M, Xie P, Kwan KY, Pang ZP, Head E, Liu Y, Hart RP, Jiang P (2022) Type-I-interferon signaling drives microglial dysfunction and senescence in human iPSC models of Down syndrome and Alzheimer's disease. Cell Stem Cell 29:1135-1153.e8. https://doi.org/10.1016/j.stem.2022.06.007
25. Lavin Y, Winter D, Blecher-Gonen R, David E, Keren-Shaul H, Merad M, Jung S, Amit I (2014) Tissue-resident macrophage enhancer landscapes are shaped by the local microenvironment. Cell 159:1312–1326. https://doi.org/10.1016/j.cell.2014.11.018
26. Liu Y, Walter S, Stagi M, Cherny D, Letiembre M, Schulz-Schaeffer W, Heine H, Penke B, Neumann H, Fassbender K (2005) LPS receptor (CD14): a receptor for phagocytosis of Alzheimer's amyloid peptide. Brain 128:1778–1789. https://doi.org/10.1093/brain/awh531
27. Ma C, Li B, Silverman D, Ding X, Li A, Xiao C, Huang G, Worden K, Muroy S, Chen W, Xu Z, Tso CF, Huang Y, Zhang Y, Luo Q, Saijo K, Dan Y (2024) Microglia regulate sleep through calcium-dependent modulation of norepinephrine transmission. Nat Neurosci 27:249–258. https://doi.org/10.1038/s41593-023-01548-5
28. Martinez A, Hériché J-K, Calvo M, Tischer C, Otxoa-de-Amezaga A, Pedragosa J, Bosch A, Planas AM, Petegnief V (2023) Characterization of microglia behaviour in healthy and pathological conditions with image analysis tools. Open Biol 13:220200. https://doi.org/10.1098/rsob.220200
29. Miyamoto A, Wake H, Ishikawa AW, Eto K, Shibata K, Murakoshi H, Koizumi S, Moorhouse AJ, Yoshimura Y, Nabekura J (2016) Microglia contact induces synapse formation in developing somatosensory cortex. Nat Commun 7:12540. https://doi.org/10.1038/ncomms12540
30. Montagni E, Resta F, Tort-Colet N, Scaglione A, Mazzamuto G, Destexhe A, Pavone FS, Mascaro ALA (2024) Mapping brain state-dependent sensory responses across the mouse cortex. iScience 27:109692. https://doi.org/10.1016/j.isci.2024.109692
31. Nakai N, Sato M, Yamashita O, Sekine Y, Fu X, Nakai J, Zalesky A, Takumi T (2023) Virtual reality-based real-time imaging reveals abnormal cortical dynamics during behavioral transitions in a mouse model of autism. Cell Rep 42:112258. https://doi.org/10.1016/j.celrep.2023.112258
32. Nimmerjahn A, Kirchhoff F, Helmchen F (2005) Resting microglial cells are highly dynamic surveillants of brain parenchyma in vivo. Science 308:1314–1318. https://doi.org/10.1126/science.1110647
33. Pachitariu M, Stringer C, Dipoppa M, Schröder S, Federico Rossi L, Dalgleish H, Carandini M, Harris KD (2017) Suite2p: beyond 10,000 neurons with standard two-photon microscopy. bioRxiv 061507
34. Paolicelli RC, Bolasco G, Pagani F, Maggi L, Scianni M, Panzanelli P, Giustetto M, Ferreira TA, Guiducci E, Dumas L, Ragozzino D, Gross CT (2011) Synaptic pruning by microglia is necessary for normal brain development. Science 333:1456–1458. https://doi.org/10.1126/science.1202529
35. Paolicelli RC, Sierra A, Stevens B, Tremblay M-E, Aguzzi A, Ajami B, Amit I, Audinat E, Bechmann I, Bennett M, Bennett F, Bessis A, Biber K, Bilbo S, Blurton-Jones M, Boddeke E, Brites D, Brône B, Brown GC, Butovsky O, Carson MJ, Castellano B, Colonna M, Cowley SA, Cunningham C, Davalos D, De Jager PL, de Strooper B, Denes A, Eggen BJL, Eyo U, Galea E, Garel S, Ginhoux F, Glass CK, Gokce O, Gomez-Nicola D, González B, Gordon S, Graeber MB, Greenhalgh AD, Gressens P, Greter M, Gutmann DH, Haass C, Heneka MT, Heppner FL, Hong S, Hume DA, Jung S, Kettenmann H, Kipnis J, Koyama R, Lemke G, Lynch M, Majewska A, Malcangio M, Malm T, Mancuso R, Masuda T, Matteoli M, McColl BW, Miron VE, Molofsky AV, Monje M, Mracsko E, Nadjar

A, Neher JJ, Neniskyte U, Neumann H, Noda M, Peng B, Peri F, Perry VH, Popovich PG, Pridans C, Priller J, Prinz M, Ragozzino D, Ransohoff RM, Salter MW, Schaefer A, Schafer DP, Schwartz M, Simons M, Smith CJ, Streit WJ, Tay TL, Tsai L-H, Verkhratsky A, von Bernhardi R, Wake H, Wittamer V, Wolf SA, Wu L-J, Wyss-Coray T (2022) Microglia states and nomenclature: a field at its crossroads. Neuron 110:3458–3483. https://doi.org/10.1016/j.neuron.2022.10.020

36. Parkhurst CN, Yang G, Ninan I, Savas JN, Yates JR 3rd, Lafaille JJ, Hempstead BL, Littman DR, Gan W-B (2013) Microglia promote learning-dependent synapse formation through brain-derived neurotrophic factor. Cell 155:1596–1609. https://doi.org/10.1016/j.cell.2013.11.030
37. Park J-C, Han JW, Lee W, Kim J, Lee S-E, Lee D, Choi H, Han J, Kang YJ, Diep YN, Cho H, Kang R, Yu WJ, Lee J, Choi M, Im S-W, Kim J-I, Mook-Jung I (2024) Microglia gravitate toward amyloid plaques surrounded by externalized phosphatidylserine via TREM2. Adv Sci (Weinh) 11:e2400064. https://doi.org/10.1002/advs.202400064
38. Pinto B, Morelli G, Rastogi M, Savardi A, Fumagalli A, Petretto A, Bartolucci M, Varea E, Catelani T, Contestabile A, Perlini LE, Cancedda L (2020) Rescuing over-activated microglia restores cognitive performance in juvenile animals of the Dp(16) mouse model of Down syndrome. Neuron 108:887-904.e12. https://doi.org/10.1016/j.neuron.2020.09.010
39. Schafer DP, Lehrman EK, Kautzman AG, Koyama R, Mardinly AR, Yamasaki R, Ransohoff RM, Greenberg ME, Barres BA, Stevens B (2012) Microglia sculpt postnatal neural circuits in an activity and complement-dependent manner. Neuron 74:691–705. https://doi.org/10.1016/j.neuron.2012.03.026
40. Schmidt U, Weigert M, Broaddus C, Myers G (2018) Cell detection with star-convex polygons. Medical image computing and computer assisted intervention—MICCAI 2018. Springer International Publishing, Cham, pp 265–273
41. Scott BB, Thiberge SY, Guo C, Tervo DGR, Brody CD, Karpova AY, Tank DW (2018) Imaging cortical dynamics in GCaMP transgenic rats with a head-mounted widefield macroscope. Neuron 100:1045-1058.e5. https://doi.org/10.1016/j.neuron.2018.09.050
42. Sierra C, De Toma I, Cascio LL, Vegas E, Dierssen M (2021) Social factors influence behavior in the novel object recognition task in a mouse model of Down Syndrome. Front Behav Neurosci 15:772734. https://doi.org/10.3389/fnbeh.2021.772734
43. Sipe GO, Lowery RL, Tremblay M-È, Kelly EA, Lamantia CE, Majewska AK (2016) Microglial P2Y12 is necessary for synaptic plasticity in mouse visual cortex. Nat Commun 7:10905. https://doi.org/10.1038/ncomms10905
44. Tiberi A, Borgonovo G, Testa G, Pacifico P, Jacob A, Di Caprio M, Totaro V, Calvello M, Cattaneo A, Capsoni S (2024) Reversal of neurological deficits by painless nerve growth factor in a mouse model of Rett syndrome. Brain 147:122–134. https://doi.org/10.1093/brain/awad282
45. Tiberi A, Carucci NM, Testa G, Rizzi C, Pacifico P, Borgonovo G, Arisi I, D'Onofrio M, Brandi R, Gan W-B, Capsoni S, Cattaneo A (2023) Reduced levels of NGF shift astrocytes toward a neurotoxic phenotype. Front Cell Dev Biol 11:1165125. https://doi.org/10.3389/fcell.2023.1165125
46. Tremblay R, Lee S, Rudy B (2016) GABAergic interneurons in the neocortex: from cellular properties to circuits. Neuron 91:260–292. https://doi.org/10.1016/j.neuron.2016.06.033
47. Villa A, Gelosa P, Castiglioni L, Cimino M, Rizzi N, Pepe G, Lolli F, Marcello E, Sironi L, Vegeto E, Maggi A (2018) Sex-specific features of microglia from adult mice. Cell Rep 23:3501–3511. https://doi.org/10.1016/j.celrep.2018.05.048
48. Wan Y, Feng B, You Y, Yu J, Xu C, Dai H, Trapp BD, Shi P, Chen Z, Hu W (2020) Microglial displacement of GABAergic synapses is a protective event during complex febrile seizures. Cell Rep 33:108346. https://doi.org/10.1016/j.celrep.2020.108346
49. Weinhard L, di Bartolomei G, Bolasco G, Machado P, Schieber NL, Neniskyte U, Exiga M, Vadisiute A, Raggioli A, Schertel A, Schwab Y, Gross CT (2018) Microglia remodel synapses by presynaptic trogocytosis and spine head filopodia induction. Nat Commun 9:1228. https://doi.org/10.1038/s41467-018-03566-5
50. Yu T, Zhang X, Shi H, Tian J, Sun L, Hu X, Cui W, Du D (2019) P2Y12 regulates microglia activation and excitatory synaptic transmission in spinal lamina II neurons during neuropathic pain in rodents. Cell Death Dis 10:165. https://doi.org/10.1038/s41419-019-1425-4
51. Zerbi V, Pagani M, Markicevic M, Matteoli M, Pozzi D, Fagiolini M, Bozzi Y, Galbusera A, Scattoni ML, Provenzano G, Banerjee A, Helmchen F, Basson MA, Ellegood J, Lerch JP, Rudin M, Gozzi A, Wenderoth N (2021) Brain mapping across 16 autism mouse models reveals a spectrum of functional connectivity subtypes. Mol Psychiatry 26:7610–7620. https://doi.org/10.1038/s41380-021-01245-4
52. Zerbi V, Pagani M, Markicevic M, Matteoli M, Pozzi D, Fagiolini M, Bozzi Y, Galbusera A, Scattoni ML, Provenzano G, Banerjee A, Helmchen F, Basson MA, Ellegood J, Lerch JP, Rudin M, Gozzi A, Wenderoth N (2022) Correction: Brain mapping across 16 autism mouse models reveals a spectrum of functional connectivity subtypes. Mol Psychiatry 27:3920–3921. https://doi.org/10.1038/s41380-022-01510-0
53. Zorrilla de San MartinDonato JC, Peixoto J, Aguirre A, Choudhary V, De Stasi AM, Lourenço J, Potier M-C, Bacci A (2020) Alterations of specific cortical GABAergic circuits underlie abnormal network activity in a mouse model of Down syndrome. Elife. https://doi.org/10.7554/eLife.58731

Publisher's Note